First bispecific inhibitors of the Epidermal Growth factor receptor kinase and the NF-κB activity as novel anti-cancer agents

*Mostafa M. Hamed,[†‡] Sarah S. Darwish,[‡] Jennifer Hermann,[§] Ashraf Abadi,[‡] Matthias Engel [‖,]**

† Pharmaceutical and Medicinal Chemistry, Saarland University, Campus C2.3, and Helmholtz Institute for Pharmaceutical Research Saarland (HIPS), Campus E8.1, D-66123 Saarbrücken, Germany.
‡ Department of Pharmaceutical Chemistry, Faculty of Pharmacy and Biotechnology, German University in Cairo, Cairo 11835, Egypt.
§ Helmholtz Institute for Pharmaceutical Research Saarland (HIPS), Campus E8.1, D-66123 Saarbrücken, Germany.
‖ Pharmaceutical and Medicinal Chemistry, Saarland University, Campus C2.3, D-66123 Saarbrücken, Germany.

ABSTRACT

The activation of the NF-κB transcription factor is a major adaptive response induced upon treatment with EGFR kinase inhibitors, leading to the emergence of resistance in non-small cell lung cancer and other tumor types. To suppress this survival mechanism, we developed new thiourea quinazoline derivatives that are dual inhibitors of both EGFR kinase and the NF-κB activity. Optimization of the hit compound, identified in a NF-κB reporter gene assay, led to compound **9b**, exhibiting a cellular IC_{50} for NF-κB inhibition of 0.3 μM while retaining a potent EGFR kinase inhibition (IC_{50} = 60 nM). The dual inhibitors showed a higher potency than gefitinib to inhibit cell growth of EGFR–overexpressing tumor cell lines *in vitro* and in a xenograft model *in vivo*, while no signs of toxicity were observed. An investigation of the molecular mechanism of NF-κB suppression revealed that the dual inhibitors depleted the transcriptional co-activator CREB-binding protein from the NF-κB complex in the nucleus.

Introduction

Inhibition of the epidermal growth factor (EGF) receptor kinase–mediated signaling is a well-established strategy for the treatment of advanced stage non-small cell lung cancer (NSCLC). Retrospective analyses have reported EGFR overexpression in 62% of NSCLC cases, and its expression was correlated with a poor prognosis.[1] However, in most cases, the clinically used EGFR kinase inhibitors, such as gefitinib and erlotinib, are only effective if the tumor cells harbor a specific activating EGFR mutation which appear to preserve the ligand–dependency of receptor activation but alter the pattern of downstream signaling.[2] This EGFR mutations include mainly small in-frame deletions in exon 19, or the single point mutation L858R,[2] and are found in ~10-50% of NSCLC patients, depending on the ethnicity and the tumor subtype.[1] Of those, about 75% show a response to the small molecule inhibitors compared to ~10% in the wild-type case.[2, 3] Hence, only a minor proportion of lung cancer patients can actually profit from the treatment with EGFR inhibitors.

In addition, tumors showing an initial response to treatment with EGFR inhibitors often become resistant due to acquisition of a mutation in the ATP binding pocket of EGFR (T790M), which mainly decreases the K_m for ATP, thus out-competing the binding of gefitinib.[2, 4] Alternatively, tumor cells might activate distinct pro-survival signaling pathways, as exemplified by the amplification of MET in lung cancers treated with EGFR inhibitors.[5]

Triple-negative breast cancer was considered another potential indication for EGFR kinase inhibitors, because they are not amenable to endocrine or ErbB2 (HER2)–directed therapies,[6] while they overexpress EGFR kinase, paralleling the loss of estrogen receptor–dependency.[7, 8] However, inhibition of EGFR by gefitinib or erlotinib showed low efficacy in arresting tumor cell growth at the cell line level, e. g. using triple-negative MDA-MB-231 cells,[9] and results

from clinical trials were disappointing.[10] Nonetheless, cell line studies showed that besides EGFR overexpression, the transcription factor NF-κB becomes constitutively active in ER–negative breast cancer cells, thus ensuring cell survival in spite of EGFR inhibition. Indeed, some evidence suggested that an additive or synergistic effect could be expected from a simultaneous inhibition of both EGFR kinase and the NF-kB pathway in triple-negative breast cancer cells.[11, 12] Notably, a crucial role of NF-κB in ensuring cell survival was also reported for other tumor types that overexpress EGFR kinase, in particular lung tumors but also head and neck squamous cell carcinomas (reviewed in [13]). Using lung cancer cell lines, a large siRNA screen identified the NF-κB pathway activity as a key factor that determined the sensitivity towards EGFR inhibitors. In the same study, knockdown of several components of the NF-κB pathway enhanced cell death induced by EGFR inhibition.[14] These findings were further validated in EGFR–dependent tumor models, confirming that the activation of NF-κB signaling conferred resistance to EGFR inhibitors and, conversely, that NF-κB knockdown enhanced sensitivity to the latter.[14] Furthermore, it was recently shown that in EGFR–mutant lung adenocarcinoma from patients, initial EGFR inhibitor treatment led to a rapid engagement of NF-κB signaling, which promoted tumor cell survival and residual disease.[15] In this study, direct pharmacologic NF-κB inhibition prevented the EGFR inhibitor–induced adaptive response, thus suppressing the emergence of EGFR inhibitor therapy resistance in several NSCLC models and in a patient–derived xenograft *in vivo*. These findings demonstrated that NF-κB activation is a critical adaptive survival mechanism engaged by EGFR oncogene inhibition and provided a rationale for EGFR and NF-κB co-inhibition to eliminate residual disease and to extend the duration of patient responses.

While co-administration of anti-tumor therapeutics is a common strategy in several current cancer trials and has proven to be beneficial in some cases, toxic side effects could increase by the number of different agents.[16] Moreover, the individual pharmacokinetic properties render it difficult to deliver effective amounts of multiple therapeutics to the tumor cells in a concerted manner to achieve maximum efficacy. Therefore, it would be a major advantage to combine the desired pharmacological activities in a single agent, in order to simultaneously suppress the synergistic EGFR and NF-κB signaling pathways at the same time. In the following, we describe the development of dual inhibitors of EGFR kinase and the NF-κB transcriptional activity based on the 4-aminophenylquinazoline scaffold, followed by an investigation of the mechanism of NF-κB suppression. Eventually, we provide first evidence for the efficacy of the novel anti-cancer agents *in vivo*.

Results and Discussion

Identification of hits displaying dual EGFR and NF-κB inhibitory activity.

With respect to EGFR kinase inhibition, it was known from previous studies that the 4-aminophenylquinazoline motif is both essential and sufficient to mediate strong inhibition of the kinase in the nM range.[17, 18] On the other hand, the 6- and 7-positions of the quinazoline scaffold offered possibilities for substitutions without strongly compromising the EGFR–directed potency, because these positions pointed towards the outside of the ATP binding pocket (compare e.g., PDB 2ITY). Of note, the quinazoline heterocycle was successfully used as a scaffold for the synthesis of potent inhibitors for a range of enzymes besides protein kinases, including endothelin converting enzyme,[19] thymidylate synthase,[20] trypanothione reductase,[21] phosphodiesterases,[22, 23] glucocerebrosidase,[24] and G9a-like protein lysine methyltransferase.[25] Hence, the quinazoline system can be considered a "privileged scaffold" according to Evans et al.[26], thus potentially suitable to serve as an affinity anchor in inhibitors of diverse enzymes – without evidence of promiscuous binding. Thus, there was some chance that new 4-aminophenylquinazoline derivatives – which are likely to retain EGFR inhibitory properties – would also inhibit one of the steps in the NF-κB activation cascade. Accordingly, a set of appropriate derivatives was prepared by us, supplemented by compounds from previous studies,[27, 28] and screened for inhibitory activity on the NF-κB activation pathway using a luciferase–based reporter gene assay. The compounds selected for the screening included derivatives with variable substitutions at the N^4-position of the aminoquinazoline nucleus, such as haloanilines, alkylanilines, alkoxyanilines, sulfonamide containing anilines and alicyclic amines (Chart 1, **I-II**). Another set of compounds featured at the 6-position different combinations of linkers, potentially acting as a H-bond donor/acceptor pair, as well as aliphatic

or (hetero)aromatic moieties which may be accommodated in potential hydrophobic binding pockets of new target proteins. In this compound set, *m*-bromoaniline was kept constant at position 4. The linker types connecting different substituents (R in Chart 1) to the quinazoline nucleus comprised imine (**III**), amide (**IV**), amino alkyl amide (**V**) and thiourea (**VI**) groups (Chart 1; the structures of all screened compounds are shown in Chart S1, Supporting Information).

The reporter gene assay was performed using the lymphoma cell line U937. Due to its origin from tissue macrophages,[29] this cell line responds with a strong activation of the NF-κB pathway after stimulation by LPS or TNFα. Inhibition of any of the essential components of the conserved classical (canonical) NF-κB pathway would be expected to result in a decrease of the final luciferase activity–based read out. Moreover, it was of importance that the U937 lymphoma cell type lacks expression of EGFR, thus excluding any interference due to the intrinsic EGFR inhibitory activity of the compounds.

Indeed, screening of the 4-anilinoquinazoline derivatives at 10 μM led to the identification of several compounds which suppressed the NF-κB reporter gene activity in U937 cells at variable degrees (Table 1; IC_{50}s were calculated for the compounds showing more than 80 % inhibition). The most potent hit was the benzylthiourea derivative **VIa**, exhibiting almost 100 % reduction of the luciferase read out (Table 1). In comparison, the reference compound gefitinib showed a considerably weaker inhibition of about 50 % at 10 μM, suggesting that the structural variations had created a significant inhibitory activity on the NF-κB pathway. Importantly, **VIa** still retained a nM potency with respect to EGFR inhibition, though it was about four times reduced compared to gefitinib (Table 1). It is worth mentioning that 4-phenethylaminoquinazoline derivatives were previously reported to inhibit the NF-κB activation in Jurkat cells, [30, 31]

however, the substitution pattern and the obtained SAR were different; in particular, an ethylene spacer between the quinazoline C(4) amino function and the phenyl ring was essential for NF-κB inhibition, which would be incompatible with EGFR kinase inhibition.[17] In contrast, the 4-aniline analog was inactive towards NF-κB, suggesting the involvement of another target. However, the mechanism of NF-κB inhibition was not investigated.

Screening of hit compound VIa against kinases directly involved in TNFα Receptor signalling.

At this stage, it was straightforward to screen the most potent hit, **VIa**, against a panel of kinases specifically involved in NF-κB activation in U937 cells,[32] in order to test whether selective inhibition of one of those kinases was responsible for the novel activity. Only one kinase in the panel shown in Table 2, RIPK-2, was weakly inhibited by **VIa**; however, with the estimated IC_{50} above 10 μM at an ATP concentration of 5 μM in the assay, RIPK-2 was unlikely to be a target of this compound in cells. Thus, we could conclude that compound **VIa** did not affect a kinase which is directly involved in TNFα receptor signaling. The results also showed that **VIa** did not exhibit non-selective kinase inhibition, which encouraged us to carry out an optimization of the potency guided by the NF-κB reporter gene assay.

Chemistry

The identified hit compound **VIa** was subject to optimization by a targeted synthesis of analogs. Our modifications centered on the substituents at the 4-anilino ring, the side chain attached to the thiourea linker and the thiourea linker itself (Schemes 1 and 2, Chart 2).

Synthesis of the quinazoline nucleus was done by refluxing of 5-nitro-2-aminobenzonitirile with triethyl orthoformate in presence of drops of acetic anhydride to yield the formimidate derivative **1**. Cyclization to form the quinazoline nucleus took place by refluxing of **1** with different anilines in acetic acid to yield the nitroquinazoline derivatives **2a-q**. Reduction of the nitro intermediates **2a-q** to their amino derivatives **3a-q** was done by refluxing the nitro derivatives with stannous chloride in methanol under nitrogen atmosphere. The benzyl thiourea derivatives **4a-4p and VIa** were obtained by stirring the aminoquinazoline derivatives **3a-q** with benzylisothiocyanate in DMF (Scheme 1).

Reaction of compound **3q** with thiophosgene yielded the isothiocyanate derivative **5** which upon stirring with different amines in DMF gave the thiourea derivatives **6a-q** and **7a-e** (Scheme 2). The N^4-(3-chlorophenyl) analogs of the later optimization campaign were synthesized in a similar manner (Scheme 3). The urea derivatives **8a-b** were obtained by stirring compound **3q** with different isocyanate derivatives in DMF (Scheme 2).

Optimization of hit VIa as dual inhibitors of both EGFR kinase and NF-κB activity.

The optimization of the hit compound included three parts. The first part was concerned with the modifications of the substituents on the 4-anilino ring while keeping the benzylthiourea at position 6 of the quinazoline (Chart 2, **4a-p**). The second part focused on modifications in the side chain linked to the thiourea moiety while keeping the 3-bromoaniline at position 4 of the quinazoline (Chart 2, compound classes **6a-q** and **7a-e**). The last part was to confirm the importance of the thiourea group by replacing it with the urea moiety (Chart 2, **8a-b**).

First, benzyl thiourea derivatives (**4a-p)** according to route A were explored (Chart 2). It was found that lipophilic substituents were highly preferred at the aniline ring, as the presence of polar groups impaired the activity. This was clearly seen with polar substituents such as the

hydroxy (**4k** and **4l**), sulfonamide (**4m**), substituted sulfonamide (**4n** and **4o**) or even the bioisosteric pyridine (**4p**), which all exhibited markedly reduced NF-κB inhibitory activity (Table 3). It was unlikely that this was only due to decreased cell permeability. Rather, the uniform reduction of activity with the more polar moieties suggested that the 4-aminophenyl is not only important for the potency toward EGFR kinase (see SAR discussion below) but also seemed to interact with the unknown target(s) in the NF-κB pathway. With respect to the lipophilic *meta*-substituents on the aniline ring, it was found that the halogens were most favorable, with chlorine giving the highest NF-κB inhibitory activity (**4c**). This was followed by bromine (**VIa**), ethyl (**4f**), methyl (**4d**) and finally the 2,3-dimethyl (**4e**). Interestingly, the bromo substituent was tolerated in the *ortho*-, *meta*- and *para*-position (**4a**, **VIa** and **4b**, respectively), with a slight preference for the *para*-position. However, this was only true for the NF-κB suppression, whereas binding to EGFR strictly demanded the bromine to be in *meta* (**VIa**, Table 3, see discussion below). For the NF-κB inhibitory activity, the *para* position tolerated even more bulky groups, such as *t*-butyl (**4h**) and phenyl (**4i**), however, no further gain of activity could be achieved compared with the halogens.

The potency of EGFR inhibition was more critically dependent on the position of the substituents in the aniline ring. It was found that (i) the *meta* position was optimum for substitutions and (ii) that the substituents must be hydrophobic. Hence, fortunately, the SAR trend paralleled that of the NF-κB inhibition. Halogens provided the highest increase in potency, in particular chlorine (**4c**), which was slightly superior to bromine in the hit compound (**VIa**). Replacing the halogen by an alkyl group such as the methyl (**4d**) decreased the activity, which further dropped with the polar hydroxyl group (**4k**). The aminophenyl binding pocket in EGFR was completely filled by the *meta*-methylated derivative **4d**, whereas the more bulky ethyl group

(**4f**) was less tolerated. Moreover, any substitutions in the *ortho*-position as in **4a** or **4e** resulted in a significantly decreased activity. Furthermore, all *para*-substitutions on the aniline also seemed to produce a steric clash with the binding pocket, irrespective to the nature of the substituent (cf. **4b**, **4g**–**j**, **4l**–**o**). Based on the sufficiently large overlap of the initial SAR, we concluded that optimization of the NF-κB inhibitory activity should be possible without loss of EGFR inhibition.

Next we tested whether the methylene spacer between the thiourea linker and the aromatic ring was required. This was done by replacing the benzyl group as in **VIa** and **7c** by phenyl, leading to **6a** and **6d**, respectively (route B in Chart 2). As can be seen in Table 4, the non-substituted benzyl/phenyl pair **VIa**/**6a** showed comparable biological activities, whereas in the case of the *p*-chloro substituted matched pair **7c** and **6d**, the *p*-chorophenyl analog **6d** was more potent than its benzyl homolog against both targets. This result suggested that the methylene group could be omitted without loss of activity and that the phenyl derivatives offered a higher potential for optimization.

Furthermore, the importance of the thiourea group was explored by a direct comparison of the thiourea derivatives **VIa** and **6d** with their urea analogues **8a** and **8b** (route C, Chart 2). It became evident that the thiourea moiety was required for the activity toward the NF-κB pathway (Table 4) but not for EGFR inhibition. The urea motif gave more potent EGFR kinase inhibitors in case of the benzyl substituent (cf. **8a** *vs*. **VIa**), however, the urea and thiourea derivatives were equipotent in case of the phenyl substituent (cf. **8b** *vs*. **6d**).

Finally, we investigated if the aromatic ring linked to the thiourea moiety was essential for the activity. To this end, the aromatic ring was replaced by a methyl group (**7a**), a morpholino-4-carboxamide derivative (**7e**) and an ethyl morpholine (**7d**). Since the suppression of the reporter

gene activity was much stronger with the benzyl (**VIa**) and phenyl (**6d**) analogs, it was concluded that the aromatic system significantly contributed to the NF-κB inhibitory activity (Table 4).

Given that a *p*-chlorine substituent in **6d** was well tolerated, several substituents were added to the phenyl thiourea side chain in an attempt to further enhance the NF-κB inhibitory potency. Firstly, we introduced several polar groups or heteroatoms in the phenyl ring (compounds **6e**, **6f**, **6g** and **7b**), which all abolished the activity toward the NF-κB pathway in the U973 cells, except the hydroxyl group (**6e**) (Table 4); however, since phenolic compounds are known to affect NF-κB signaling by various, often non-specific mechanism,[33] this derivative was not further pursued. Hence we decided to switch to lipophilic substituents (compounds **6b-6d, 6h-6q**, Scheme 2); this modification resulted in sharp SAR, as indicated by highly variable activities depending on the size and the position of the substituents (compounds **6b-6d, 6h-6q**, Table 4). Concerning the EGFR kinase inhibition, diverse substituents of either lipophilic or hydrophilic nature were tolerated, with the hydrophilic or heterocyclic moieties being the most potent (cf. **6e**, **6f**, **7b** and **7d**). However, multiple and/or bulky lipophilic substituents on the phenyl ring (such as in **6i, 6m, 6o-6q**) decreased or abolished the activity. The latter SAR were conflicting with the requirements for potent inhibition of NF-κB activation, thus it was not possible to optimize both biological activities in parallel to the same degree. Altogether, compounds **6c** and **6h** showed the best balance between EGFR inhibition and simultaneous suppression of the NF-κB activation in the reporter gene assay (Table 4).

The reference compound gefitinib, which is in clinical use for the treatment of NSCLC, was only moderately active against NF-κB in the reporter gene assay (Table 4), confirming that the inhibition of EGFR kinase was not responsible for the suppression of the NF-κB activity in the

U937 cells. Moreover, several of the new compounds were considerably more potent in the inhibition of NF-κB, despite of displaying lower EGFR kinase inhibition (cf. **6h**, **6j** and **6l** in Table 4).

Inhibition of MDA-MB-231 breast cancer cell growth.

Next, we evaluated whether the dual inhibitory activity of the novel quinazoline derivatives boosts the efficacy as potential anti-tumor agents compared with EGFR inhibition alone. The breast cancer cell line MDA-MB-231 was chosen because it was frequently used as a model for studying the effects of EGFR inhibition in triple-negative breast cancer cells.[9, 11, 34] Like many clinical triple-negative tumors, MDA-MB-231 cells are rather insensitive to the EGFR inhibitor gefitinib (reported IC_{50} range for cell growth inhibition: 15-20 μM), in spite of the strong overexpression of EGFR kinase.[9, 35] In addition, this cell line displays constitutive activation of NF-κB,[11, 12] which is a frequent feature found in most breast cancer tumors.[36]

Hence, any superior efficacy of our novel compounds should be easily detectable using this cell line. The results of the MTT assay are included in Tables 3 and 4; notably, two of the new compounds inhibited MDA-MB-231 cell growth more than 35 times stronger than the reference compound gefitinib (cf. **6h**, **6j**). Our data further indicated that, as a general trend, the potency to suppress MDA-MB-231 cell growth was determined by the NF-κB inhibitory activity rather than by the potency of EGFR kinase inhibition. This was obvious from the fact that, with the exception of **6n**, the most potent inhibitors of the NF-κB activation in U937 cells were also the strongest inhibitors of the MDA-MB-231 cell growth (cf. **6c**, **6h, 6i, 6j**, **6l** and **6m** in Table 4), the more since among these, **6i**, **6j** and **6m** showed only low potency against EGFR kinase. *Vice versa*, several congeners showing a high activity toward EGFR kinase (**VIa**, **6a**, **6b**, **6d**, **6e**, **6f**, **7a**, **7b**, **7d** and **8a**), that were among the least potent inhibitors of NF-κB activation, inhibited the

MDA-MB-231 cell growth with only moderate to poor IC_{50}s between 8.2 and >30 μM, similarly to gefitinib. In conclusion, the suppression of the NF-κB activation was mainly responsible for the tumor cell growth inhibition.

Effects on A549 lung cancer cells *vs.* non-tumor cell lines.

The potency of the best compounds to inhibit the cell growth of the lung cancer cell line A549 was also tested. This assay was done to corroborate if the compounds with dual inhibitory activity still offer an advantage towards a cell line which is intermediately sensitive to potent EGFR inhibitors such as gefitinib. The results showed that the dual inhibitors are more potent than gefitinib in inhibiting the growth of A549 cancer cells (Table 5). Importantly, when the selected compounds were tested against non-tumor cell lines (chinese hamster ovary (CHO)-K1 and human umbilical vein endothelial cells (HUVEC)), significantly weaker effects of **6c** and **6h** on the cell growth were noted, suggesting that the compounds exerted a rather tumor cell–selective cytotoxicity (Table 5). Of note, the efficacy/toxicity window was larger for **6c** and **6h** than for gefitinib with the cell lines tested.

Kinase selectivity profile of 6c.

Since the novel dual inhibitors were developed based on a kinase inhibitor scaffold, it was straightforward to test the selectivity over other kinases and whether the suppression of the NF-κB activation was also due to inhibition of a kinase. To this end, an *in vitro* selectivity profiling was performed against a panel of 106 protein kinases, including both tyrosine and Ser/Thr kinases from each branch of the human kinome. For the profiling we selected **6c**, which had shown a slightly stronger EGFR kinase inhibition than **6h**. The screening results are summarized in Table S1 (Supporting Information). It was found that compound **6c** exhibited an excellent selectivity for the EGFR kinase, with only a weak inhibition of two other kinases, namely Mnk2

and Pim-1. The IC_{50}s for these two kinases were determined to be 2.7 and 1.2 μM, respectively. In the same assay campaign, the IC_{50} for EGFR kinase was 41 nM (Table S2, Supporting Information). Interestingly, **6c** appeared to be more selective than gefitinib, as the latter had inhibited in a previously reported screening the kinases Mnk2, SIK2, Mnk1, LOK/STK10, ErbB2/HER2, RIPK2, EPHA6, ErbB4/HER4 by 46 to 76 % at 0.5 μM (Supplementary Table S3 in Ref. [37]). From these kinases, Mnk2, LOK, RIPK2 and ErbB4 were also present in the panel screened with **6c**, but only Mnk2 and ErbB4 were appreciable inhibited, by 78 % and 54 %, respectively, however at a ten times higher concentration (5 μM). The cell-free potency of **6c** for Mnk2 inhibition appeared too low to explain the efficacy of **6c** in the cell–based NF-κB reporter gene assay (IC_{50} = 1.9 μM). Moreover, gefitinib displayed a higher off-target inhibition of Mnk2[37] than **6c**, but was less potent in our reporter gene assay. Thus, Mnk2 could be excluded as a potential target of the dual inhibitors in the NF-κB activation pathway. The inhibition of Pim-1 by **6c** was also rather weak, nevertheless we decided to check the potential role of Pim-1 in the NF-κB activation pathway using the potent Pim-1 inhibitor SIM-4a (IC_{50} for Pim-1: 17 nM at 100 μM ATP in the cell-free assay [38]). Testing SIM-4a in the NF-κB reporter gene assay in concentrations from 1 to 5 μM, we could not detect any inhibition (Table S3, Supporting Information), ruling out Pim-1 as a target of **6c** in the NF-κB activation pathway.

In light of the remarkable selectivity of compound **6c**, it was rather unlikely that the new biological target was another protein kinase, although it could not be fully excluded since not the complete kinome was screened. However, if it was a kinase, then it would be part of an unknown NF-κB activation pathway that is also induced by TNFα, because all kinases identified as part of the TNFα receptor complex[32] had been included in the kinase screen, also all other kinases which had previously been mentioned in literature to play a role in NF-κB activation.

Elucidation of the mechanism of action responsible for NF-κB suppression. 6c and 6h do not inhibit the cellular proteasome.

Having developed novel dual inhibitors, we aimed at investigating the cellular mechanism of action which was responsible for the observed suppression of NF-κB activation in the reporter gene assay, assuming that it was not the inhibition of another kinase. The most obvious biological activity to test was the potential inhibition of the cellular 26S proteasome, which is essential for the degradation of the inhibitory protein IκB.[39] The prototype of proteasome inhibitors, bortezomib, inhibits mainly two of the three distinct proteolytic activities, thus preventing the release of the NF-κB dimer.[40]

For each of the three proteolytic activities, the trypsin-like, the chymotrypsin-like, and the caspase-like, we used a specific fluorigenic peptide and total protein extract from MDA-MB-231 cells as a source of proteasomal activities, basically as described.[41] However, whereas Bortezomib fully inhibited all three proteolytic activites at 1 μM, none of the test compounds showed any inhibitory activity even at 50 μM (data not shown). Thus, the three main proteolytic activities of the proteasome could be excluded as molecular targets.

6c and 6h do not inhibit translocation of NF-κB/p65 to the nucleus.

It was theoretically possible that the compounds caused the cytoplasmic retention of the NF-κB dimer through an alternate mechanism; hence we analyzed whether the translocation of the RelA subunit (p65) of NF-κB was affected. To this end, we used a high-content screening system employing a CHO cell line stably expressing a GFP-p65 fusion protein. A cytoplasmic retention of this construct in the presence of the test compounds, as indicated by a diffuse cytoplasmic fluorescence, would signify an inhibition of the upstream NF-κB activation. The system automatically quantifies the ratio of cytoplasmic vs. nuclear fluorescence and provides

microphotographs of each well. The cells were first stimulated for 30 min by 25 ng/mL IL-1β after which the translocation of the GFP-NFκB-p65 fusion protein from the cytoplasm to the nucleus was visualized. Bortezomib was used as a positive control, and gefitinib was also included for comparison. While bortezomib clearly prevented the migration of the NF-κB construct to the nucleus in a concentration–dependent manner, **6c**, **6h** and gefitinib were completely inactive (Figure S1, Supporting Information). To make sure that the lack of activity of the phenylthiourea derivatives was not due to solubility problems under the conditions used, Pluronic F-127 (indicated by "P") was added in some experiments to increase the solubility at higher concentrations; however, this did not change the outcome (Figure S1).

Compound 6c does not influence DNA binding of NF-κB/p65.

Having ruled out that the dual inhibitors prevented the translocation of NF-κB/p65 to the nucleus, it was tempting to speculate that the DNA binding activity of the NF-κB complex was affected by the compounds. To investigate this possibility, the DNA binding capability of the NF-κB species in nuclear protein extracts isolated from MDA-MB 231 cells was analyzed using a commercial ELISA kit. This assay relied on measurement of the specific binding to the NF-κB response element oligonucleotide immobilized in a 96 well plate. The experiment was performed in two different ways: (i) MDA-MB 231 cells were incubated with **6c** for 12 h, followed by washing of the cells, isolation of the nuclear proteins and DNA-binding analysis, and (ii) nuclear extracts were prepared from untreated cells and the DNA-binding quantified in the presence of **6c** *vs.* DMSO. Method (i) would allow detecting any compound–induced, intrinsic down-regulation of the DNA-binding activity, whereas variant (ii) would identify a direct inhibition of DNA-binding. The results of our experiments showed that **6c** did not impair the DNA-binding

activity of the NF-κB complexes in the nuclear extract, neither directly nor *via* modulation of regulatory mechanisms (Figure S2, Supporting Information).

Compound 6c reduces the amount of CREB-binding protein (CBP) in the NF-κB transcription factor complex.

One of the few remaining possibilities was that the new inhibitors interfere with the NF-κB activity at the level of transcriptional co-activators. It is known that, in order to become fully transcriptionally active in the nucleus, the NF-κB dimer recruits transcriptional co-activators such as the CREB-binding protein (CBP)/p300, which functions as a histone acetyl transferase.[42] Evidence from literature suggested that at least in some cell types, a CBP knockdown can cause a down-regulation of the NF-κB transcriptional activity without affecting nuclear translocation or DNA-binding affinity of NF-κB.[43, 44] Hence, we decided to analyze the amount of CBP present in the DNA-binding NF-κB complex isolated from MDA-MB-231 cells that were treated with **6c**. Indeed, we found that compound **6c** but not gefitinib reduced the amount of CBP in the NF-κB transcription complex in a concentration–dependent manner (Figure 1A). In the same samples, the amount of RelA/p65 bound to the immobilized NF-κB response element oligonucleotide was not changed by the compounds (Figure 1B). Thus, we provide first evidence that our dual inhibitors down-regulate the transcriptional activity of NF-κB through depletion of the co-activator CBP from the transcription factor complex. However, further studies are needed to elucidate the underlying mechanism.

Pharmacological disruption of the p65/CBP interaction might abolish the expression of several tumor–relevant genes. For instance, it was shown that the cooperation of p65/RelA and CBP was required for the expression of anti-apoptotic genes such as cIAP2 and XIAP in rat fibroblasts[45] as well as the pro-inflammatory cytokines IL-1β and IL-6 and CSF2 in lung cells.[44]

Thus, it seems possible that our novel dual inhibitors also suppress the NF-kB–mediated IL-6 expression in cancer cells. Of note, IL-6 was identified by Blakely et al. as the NF-κB target gene that was most significantly increased in the adaptive response to EGFR kinase inhibition by erlotinib, both at the mRNA and the protein level.[15] This adaptive response mechanism was also confirmed in resected NSCLC.[15] On the other hand, the interaction of RelA with CBP is only required for the expression of a subset of NF-κB–dependent genes,[44, 46] which might result in lower toxicity than total inhibition of NF-κB activity, e. g. as mediated by IκB kinase inhibitors.[47-49] Indeed, our *in vitro* and *in vivo* experiments suggested low toxicity against non-tumor cells and tissues (see below). Also with respect to the therapeutic outcome, total suppression of NF-κB activity is not desirable because it will also affect the anti-tumor activity of T-lymphocytes in the tumor microenvironment.[49, 50] Further studies are needed to investigate whether the thiourea quinazolines will inhibit the CBP–dependent NF-κB signaling in tumor cells sufficiently selectivity so that T cells of the M1 phentotype remain functional.

CBP is a co-activator in a multitude of transcription factor complexes; total depletion of CBP, in particular from the general transcription factors, would therefore lead to non-selective cytotoxicity, which was not observed with our dual inhibitors. This suggests a more selective modulation of CBP association by our compounds, which remains to be elucidated. Interestingly, CBP was already targeted previously by small molecules that inhibit the histone acetyltransferase activity of the protein for the therapy of leukemia.[51] These inhibitors also showed surprisingly little cytotoxicity, although besides histones, more than 100 proteins from a multitude of signaling pathways have been implicated as CBP acetylation substrates.[52]

Optimization of pharmacokinetic (PK) properties.

In order to obtain candidates for metabolic stability and *in vivo* PK studies, we aimed at further optimizing the prototype dual inhibitors **6c** and **6h**. To this end, the most favourable compound features as identified in the initial phase were combined in order to increase the potency toward the NF-κB pathway. In addition, since this could result in predominantly lipophilic compounds, we aimed at enhancing the PK properties and druglikeness in parallel. As described above, a chlorine or bromine atom in the *meta* position of the 4-anilino ring was favorable for the NF-κB inhibitory activity (cf. **4c** and **VIa**, respectively, Table 3). Hence we decided to uniformely incorporate *m*-chloro due to the smaller size and more moderate impact on logP compared with bromine. It was furthermore favorable for the potency to include a lipophilic aromatic system on the thiourea group. Also considering metabolic stability issues, the chlorine as present in compounds **6c** and **6h** was replaced by fluorine (**9a** and **9b**). While the 3,4-difluorophenyl moiety led to reduced activities both in the NF-κB reporter gene and the EGFR kinase assay (**9a**), the 3,5-difluoro substitution (**9b**) favorably increased the potency to suppress the activation of NF-κB (IC_{50} = 0.3 μM, Table 6) compared with **6c** and **6h** (IC_{50}s: 1.9 and 1.0 μM, respectively). In addition, the inhibitory potency toward EGFR kinase was still in the nanomolar range (IC50 = 60.1 nM). The last set of compounds aimed at the enhancement of water solubility through replacing the thiourea–linked phenyl by different N-heterocycles, comprising pyridine (**9c**), thiazole (**9d** and **9e**) and thiadiazole (**9f** and **9g**). To maintain a suitable balance between polarity and lipophilicity, all heterocyclic rings were decorated with a lipophilic substituent. The 3-chloropyridine (**9c**) and the electron–rich 5-membered heterocycles had a distinct influence on the dual activity when compared with **6c**: while the pyridine ring slightly decreased both biological activities to a similar extent, the thiazole and thiadiazole rings reduced the potency against EGFR kinase by about 5-6 fold (**9d**-**9g**, Table 6). On the other hand, the latter

compounds showed preserved or even enhanced activity against the NF-κB pathway, with **9d** and **9e** exhibiting sub-micromolar IC_{50}s. Altogether, aromatic heterocycles, in particular thiazole, were tolerated while enhancing the water solubility compared with the halogenated phenyl analogs (cf. **9d** *vs.* **6c** and **9b**, Table S4, Supporting Information).

The best compounds from this last optimization round, **9b**, **9d** and **9e** were then tested for growth inhibitory activity against MDA-MB-231 cells. While **9b** and **9d** exhibited comparable IC_{50} values (1.1 and 0.9 μM, respectively), **9e** surprisingly lacked activity against this cell line even at 20 μM. The reason for this is unclear, but it could be possible that **9e** was unstable under the prolonged cell culture conditions.

In summary, **9b** showed a balanced inhibitory profile and was the most potent compound in the NF-κB reporter gene assay (IC_{50} = 0.3 μM). Since the substitution pattern of the phenyl was changed compared with **6c**, we eventually verified that this did not influence the kinase selectivity. It could be confirmed that the selectivity was retained or became even superior to **6c**, as indicated by the weaker inhibition of Pim-1 and ErbB4 compared with **6c** (Table S5).

The 4-(trifluoromethyl)thiazolyl analog **9d** also exhibited a good NF-κB inhibitory activity (IC_{50} = 0.6 μM) and efficiently inhibited MDA-MB-231 cell growth, although the activity toward purified EGFR kinase was decreased (IC_{50} = 137 nM). However, since the potency to suppress MDA-MB-231 cell growth was mainly determined by the NF-κB inhibitory activity (cf. above), both **9b** and **9d** were selected as candidates for pharmacokinetic studies.

Pharmacokinetic evaluation *in vitro* and ***in vivo*.**

First, the lead compounds **9b** and **9d** were evaluated for their phase I metabolic stability using rat liver microsomes. Samples were taken at defined time points, and the remaining percentage of parent compound was determined by LC-MS/MS. Half-life and intrinsic clearance were

calculated for the test compound and the two reference compounds diazepam and diphenhydramine (Table 7). Although **9d** was considerably less stable than **9b**, reaching only the half-life and predicted clearance of diphenhydramine, it was conceivable that this disadvantage might be compensated by the higher water solubility (Table S4, Supporting Information). In contrast, **9b** displayed higher stability in the microsomal assay than the reference drug diazepam, however, there was only a slight improvement of the water solubility compared with **6c** (Table S4). Because of their complementary properties, **9d** and **9b** were both included in the *in vivo* PK study. As shown in Figure 2 and Table 8, **9b** showed a good plasma half-life of about 7.8 h, and the compound was not completely eliminated after 24 h. Despite the lower water solubility, the AUC of **9b** was more than 5-times higher than that of **9d** (Table S4). This was partially attributable to the more rapid liver metabolism of **9d**, however, the maximum plasma concentration (C_{max}) reached by **9d** was lower than expected with a subcutaneous injection, suggesting that further factors impaired the plasma availability. Finally, **9b** was evaluated further in a xenograft tumor model.

Tumor xenograft study.

MDA-MB-231 cells were injected under the skin of nude mice and the treatment by compounds or vehicle started after day 5 of the tumor cell inoculation. We decided to use a 10 mg/kg dose of **9b** to minimize solubility problems, and 25 mg/kg of the reference drug gefitinib. The higher dose was chosen to make sure that gefitinib would show at least some measureable effect, since the MDA-MB-231 cells were rather insensitive toward this drug (cf. Table 4).[9] In a previous study, s.c. application was demonstrated to be an efficient administration route for gefitinib in a tumor xenograft model in nude mice.[53] In addition, gefitinib exhibits higher water solubility than our compounds (cf., Table S4) and was reported to achieve high and sustained

blood levels in mice,[54] suggesting an at least comparable bioavailability of gefitinib to the transplanted tumor cells in our model.

It can be seen from Figure 3 that the lower dose of **9b** inhibited the tumor growth to the same extent as gefitinib. During the study, tumor growth was unexpectedly slow, possibly impeding the observation of more pronounced effects of the drugs. Especially in the first two weeks of treatment, the delayed growth of some tumors caused high variations of the measured sizes. The tumors then started growing stronger in the vehicle– but not in the compound–treated group, so that significant differences were reached after day 21 (Figure 3).

Absence of adverse effects *in vivo*.

In both the pharmacokinetic study (durance 24 h) and the xenograft study (treatment over 28 days), no adverse effects of **9d** and/or **9b** were observed. No anomalous behavior was seen, and the organs after killing of the animals appeared morphologically normal. The body weight was not affected by **9b** over the 28 days period. Thus, it can be concluded that the compounds were non-toxic to mice and well tolerated at the administered dose.

Conclusion

Using a serendipity approach, thiourea quinazoline derivatives showing a dual inhibitory activity towards the EGFR and the NF-κB activity were discovered. Optimization of the hit compound **VIa** resulted in **9b** and **9d** as best compounds for NF-κB inhibition with cellular IC_{50}s in the submicromolar range. We provided *in vitro* and *in vivo* evidence that tumor cells which are only weakly responsive towards EGFR inhibition can still be combatted by the novel NF-κB inhibitory activity. Compared to sole EGFR kinase inhibitors, our dual inhibitors might show higher efficacy in two scenarios: (i) The "in-built" NF-κB inhibitory activity might sensitize EGFR kinase–overexpressing, originally non-responsive tumors to EGFR kinase inhibition, and (ii) it might suppress the occurrence of resistant tumor cells, that were initially sensitive toward EGFR kinase inhibitors, but amplify NF-κB signaling as an adaptive response.[15]

The modulation of the NF-κB transcriptional activity by the thiourea quinazoline derivatives involves depletion of the co-activator CBP, which is a novel mechanism requiring in-depth characterization in future studies. At any rate, the dual inhibitors exhibited a tumor cell–selective cytotoxicity.

Based on the encouraging results from our simplified *in vivo* model, more challenging and predictive tumor models can be envisaged in the future to test the efficacy of our dual inhibitors, such as patient–derived cancer tissue xenografts, which preserve the intra-tumoral heterogeneity of primary malignancies.[55]

Experimental

Chemistry

Solvents and reagents were obtained from commercial suppliers and used as received. 1H and 13C NMR spectra were recorded on a Bruker DRX 500 spectrometer. Chemical shifts are referenced to the residual protonated solvent signals. The purities of all biologically tested compounds were determined by HPLC coupled with mass spectrometry and were higher than 95% in all cases. Mass spectrometric analysis (HPLC-ESI-MS) was performed on a TSQ quantum (Thermo Electron Corporation) instrument equipped with an ESI source and a triple quadrupole mass detector (Thermo Finnigan). The MS detection was carried out at a spray voltage of 4.2 kV, a nitrogen sheath gas pressure of 4.0 x 105 Pa, an auxiliary gas pressure of 1.0 x 105 Pa, a capillary temperature of 400 ºC, a capillary voltage of 35 V, and a source CID of 10 V. All samples were injected by an autosampler (Surveyor, Thermo Finnigan) with an injection volume of 10 μL. An RP C18 NUCLEODUR 100-3 (125 x 3 mm) column (Macherey-Nagel) was used as the stationary phase. The solvent system consisted of water containing 0.1% TFA (A) and 0.1% TFA in acetonitrile (B). HPLC-Method: flow rate 400 μL/min. The percentage of B started at an initial of 5%, was increased up to 100% during 16 min, kept at 100% for 2 min, and flushed back to 5% in 2 min. High resolution precise mass spectra were determined for compounds **6c**, **6h**, **9b**, **9d** and were recorded on ThermoFisher Scientific (TF, Dreieich, Germany) Q Exactive Focus system equipped with heated electrospray ionization (HESI)-II source and Xcalibur (Version 4.0.27.19) software. Mass calibration was done prior to analysis according to the manufacturer's recommendations using external mass calibration. All samples were constituted in methanol and directly injected onto the Q Exactive Focus using the integrated syringe pump. All data acquisition was done in positive ion mode using voltage scans and the

data collected in continuum mode. Melting points are uncorrected and were determined on Buchi melting point apparatus (B-540). The IR spectra were measured on Nicolet 380 FT-IR spectrometer.

1-benzyl-3-(4-((3-bromophenyl)amino)quinazolin-6-yl)thiourea (VIa). Yield 63%; m.p. 197-198 °C; ^{1}H NMR (500 MHz, DMSO) δ 9.91 (s, 1H), 9.83 (s, 1H), 8.64 (s, 1H), 8.47 (d, *J* = 1.3 Hz, 1H), 8.42 (s, 1H), 8.25 (t, *J* = 1.9 Hz, 1H), 7.93 (ddd, *J* = 8.2, 1.9, 0.9 Hz, 1H), 7.85 (dd, *J* = 8.9, 2.1 Hz, 1H), 7.78 (d, *J* = 8.9 Hz, 1H), 7.38 – 7.31 (m, 5H), 7.30 (ddd, *J* = 7.9, 1.9, 1.0 Hz, 1H), 7.25 (t, *J* = 7.1 Hz, 1H), 4.79 (d, *J* = 5.1 Hz, 2H). ^{13}C NMR (126 MHz, DMSO) δ 181.56, 157.11, 153.66, 147.51, 141.07, 139.00, 136.98, 131.83, 131.80, 130.41, 128.21, 127.41, 126.83, 125.86, 123.89, 121.21, 120.43, 117.77, 115.26, 47.51. MS (+ESI): m/z = 464.09 (M + H).

1-(4-((3-bromophenyl)amino)quinazolin-6-yl)-3-(3-chlorophenyl)thiourea (6c). Yield 60%; m.p. 180-182°C; ^{1}H NMR (500 MHz, DMSO) δ 10.19 (s, 1H), 10.06 (s, 1H), 9.84 (s, 1H), 8.65 (s, 1H), 8.49 (d, *J* = 1.8 Hz, 1H), 8.23 (t, *J* = 1.8 Hz, 1H), 7.94 – 7.84 (m, 2H), 7.80 (d, *J* = 8.8 Hz, 1H), 7.70 (t, *J* = 2.0 Hz, 1H), 7.43 (d, *J* = 9.0 Hz, 1H), 7.36 (td, *J* = 8.0, 4.1 Hz, 2H), 7.30 (d, *J* = 8.7 Hz, 1H), 7.20 (ddd, *J* = 7.9, 2.0, 1.0 Hz, 1H). ^{13}C NMR (126 MHz, DMSO) δ 180.49, 157.15, 153.80, 147.66, 140.96, 140.89, 137.09, 132.49, 132.03, 130.40, 130.00, 128.10, 125.95, 124.34, 124.05, 123.52, 122.43, 121.18, 120.59, 118.36, 115.13. HRMS (+ESI) m/z: $[M + H]^{+}$ Calcd for $C_{21}H_{16}BrClN_5S$ 483.99983; Found 483.99921.

1-(4-((3-bromophenyl)amino)quinazolin-6-yl)-3-(3-chloro-4-fluorophenyl)thiourea (6h). Yield 63%; m.p. 206-207°C; ^{1}H NMR (500 MHz, DMSO) δ 10.19 (s, 1H), 9.98 (s, 1H), 9.84 (s, 1H), 8.65 (s, 1H), 8.49 (d, *J* = 2.1 Hz, 1H), 8.24 (t, *J* = 2.0 Hz, 1H), 7.91 (ddd, *J* = 8.1, 2.0, 1.0 Hz, 1H), 7.86 (dd, *J* = 8.9, 2.2 Hz, 1H), 7.80 (d, *J* = 8.9 Hz, 1H), 7.77 (dd, *J* = 6.8, 2.5 Hz, 1H),

7.44 (ddd, J = 8.9, 4.6, 2.5 Hz, 1H), 7.41 (d, J = 9.0 Hz, 1H), 7.36 (dd, J = 14.2, 6.1 Hz, 1H), 7.30 (ddd, J = 8.0, 1.9, 1.0 Hz, 1H). ^{13}C NMR (126 MHz, DMSO) δ 180.77, 157.17, 154.42 (d, $^{1}J_{C\text{-}F}$ = 244.6 Hz), 153.87, 147.75, 140.98, 137.00, 136.59, 132.07, 130.41, 128.21, 126.43, 125.97, 125.20 (d, $^{3}J_{C\text{-}F}$ = 7.2 Hz), 124.05, 121.21, 120.59, 118.71 (d, $^{2}J_{C\text{-}F}$ = 18.6 Hz), 118.46, 116.47 (d, $^{2}J_{C\text{-}F}$ = 21.8 Hz), 115.18. HRMS (+ESI) m/z: $[M + H]^+$ Calcd for $C_{21}H_{15}BrClFN_5S$ 501.99041; Found 501.98968.

1-(4-((3-chlorophenyl)amino)quinazolin-6-yl)-3-(3,5-difluorophenyl)thiourea (9b). Yield 31%; m.p. 168.5-170.5°C; ^{1}H NMR (500 MHz, DMSO) δ 10.36 (s, 1H), 10.25 (s, 1H), 9.87 (s, 1H), 8.65 (s, 1H), 8.50 (d, J = 2.0 Hz, 1H), 8.11 (t, J = 1.9 Hz, 1H), 7.87 (dd, J = 8.9, 2.1 Hz, 1H), 7.84 (dd, J = 8.3, 1.2 Hz, 1H), 7.81 (d, J = 8.8 Hz, 1H), 7.42 (t, J = 8.1 Hz, 1H), 7.36 (dd, J = 9.3, 2.2 Hz, 2H), 7.17 (ddd, J = 8.0, 2.1, 0.9 Hz, 1H), 6.99 (tt, J = 9.3, 2.3 Hz, 1H). ^{13}C NMR (126 MHz, DMSO) δ 180.40, 162.03 (dd, J = 243.3, 15.3 Hz), 157.22, 153.92, 147.80, 142.17 (t, J = 13.5 Hz), 140.84, 137.00, 132.77, 132.10, 130.13, 128.18, 123.12, 121.30, 120.24, 118.50, 115.18, 106.23 (dd, J = 27.9, 6.3 Hz), 99.49 (t, J = 26.0 Hz). HRMS (+ESI) m/z: $[M + H]^+$ Calcd for $C_{21}H_{15}ClF_2N_5S$ 442.07048; Found 442.06946.

1-(4-((3-chlorophenyl)amino)quinazolin-6-yl)-3-(4-(trifluoromethyl)thiazol-2-yl)thiourea (9d). Yield 25%; m.p. 226-228°C; ^{1}H NMR (500 MHz, DMSO) δ 12.48 (s, 1H), 10.35 (s, 1H), 9.91 (s, 1H), 8.67 (s, 1H), 8.58 (d, J = 2.1 Hz, 1H), 8.10 (s, 1H), 7.95 (dd, J = 8.9, 2.2 Hz, 1H), 7.86 (d, J = 1.0 Hz, 1H), 7.84 (d, J = 8.9 Hz, 2H), 7.42 (t, J = 8.1 Hz, 1H), 7.18 (ddd, J = 8.0, 2.1, 0.9 Hz, 1H). ^{13}C NMR (126 MHz, DMSO) δ 177.95, 162.58 (q, J = 4.9, 2.7 Hz), 157.28, 154.12, 147.97, 140.74, 137.42 (q, J = 36.6 Hz), 136.24, 132.75, 131.85, 130.10, 128.25, 123.21, 121.41, 120.93 (q, J = 269.9 Hz), 120.34, 118.71, 115.55 (q, J = 3.3 Hz), 115.15. HRMS (+ESI) m/z: $[M + H]^+$ Calcd for $C_{19}H_{13}ClF_3N_6S_2$ 481.02837; Found 481.02740.

Biology

EGFR kinase phosphorylation assay. Phosphorylation assays were performed in a final volume of 20 µL containing 8 mM MOPS (pH 7.0), 0.2 mM EDTA, 10 mM $MnCl_2$, 200 µM substrate peptide, 0.25 mM DTT, 0.1 mg/mL BSA, 10 ng wild-type EGFR-Kinase (Cat. No. 40187, BPS Bioscience), 10 mM magnesium acetate, 100 µM γ–[^{32}P]ATP, and inhibitors or DMSO control (1.25% v/v). For IC_{50} curves with the wild-type enzyme, the following concentrations of the compounds (in nM) were tested in triplicates: 150, 100, 50, 25, 15, 10, 7.5, 5, 2.5. The assays were repeated at least once. Reactions were started by the addition of the magnesium acetate/ATP mixture. After 30 min incubation at 30°C, 5 µL of each reaction was spotted on phosphocellulose P81 paper (Whatman). The P81 paper was then washed 5 times with 50 mM phosphoric acid for 15 min, dried and exposed to a phosphorimager screen (Storm, GE Healthcare), which was scanned and densitometrically analyzed the next day. The sequence of the substrate peptide was derived from phospholipase C-γ1 and had the sequence "KHKKLAEGSAYEEV", according to Fry *et al.*.[56]

Reporter Gene Assay. The NF-κB reporter gene assay was performed in U937 cells exactly as previously described.[57]

MDA-MB-231 cell growth inhibition assay. Cells were seeded in 96-well standard assay microplates at a density of 45,000 cells per well, then allowed to adhere overnight before compound addition. After 24 hours, cells were treated with different concentrations of the compounds. Cells were incubated for an additional 48 hours at 37 °C, after which 20 µL of MTT reagent (prepared as 5 mg/mL PBS) were added and then incubated for additional 1 hour. After that, 100 µL SDS (prepared as 10% in 0.01 N HCl) were added and incubated for at least 2 h at

37 °C to allow for cell lysis. Absorbance was then measured at a wavelength of 570nm in a plate reader (PolarStar, BMG Labtech, Freiburg, Germany).

Cultivation of HUVEC, CHO-K1 and A549 cells for cytotoxicity assays. HUVEC cells purchased from the American Type Culture Collection (Manassas, VA) were maintained and seeded in F-12K nutrient mixture (Kaighn's modification; Life Technologies) with 10% FBS, 100 μg/mL heparin (Sigma-Aldrich, St. Louis, MO), and 30 μg/mL endothelial cell growth supplement (Sigma-Aldrich). For the MTT assay, 6 x 10^3 cells per well of 96-well plates were used. CHO-K1 cells (ACC-110) were obtained from the German Collection of Microorganisms and Cell Cultures (Deutsche Sammlung für Mikroorganismen und Zellkulturen, DSMZ) and were cultured under conditions recommended by the depositor. Cells were seeded at 6 x 10^3 cells per well of 96-well plates in 180 μL complete medium (F12K, 10% FBS). A549 cells obtained from the "Deutsche Sammlung für Mikroorganismen und Zellkulturen" (DSMZ) (ACC 107) were grown in Dulbecco's modified Eagle's medium (DMEM, Sigma) with 10 % fetal calf serum (FCS, Sigma). Cells were also seeded at 6 x 10^3 cells per well of 96-well plates.

All cell media contained in addition penicillin G (final concentration 100 U/mL) and streptomycin sulfate (final concentration 100 mg/mL), and were maintained at 37° C and 5% CO_2 in a humidified incubator. The cytotoxicity of the test compound was determined as described above, under "MDA-MB-231 cell growth inhibition assay".

NF-κB (p65)-DNA binding and p65/CREB-binding protein ELISA. MDA-MB-231 breast cancer cells were grown in 6-well plates to 80% confluency in DMEM containing 10 % FCS (low endotoxin quality, GIBCO, Thermo Fisher Scientific), and pen/strep mix. The cells were incubated with the test compounds or DMSO as solvent control for 12 h. In some experiments, TNFα was added at final concentration of 20 ng/mL (as indicated) and the incubation continued

for 20 min at 37°C. The plates were then put on ice, washed twice with ice-cold PBS and harvested in 1 mL PBS using a cell scraper (Sigma, cat. no. CLS3010). The suspension was transferred to Eppendorf tubes on ice, and the cells were spun down at 500 g in a cooled centrifuge (2° C). Nuclear protein extracts were immediately prepared using the Pierce NE-PER Nuclear and Cytoplasmic Extraction Kit (Thermo Fisher Scientific, cat. no. PI-78833) according to the manufacturer´s instructions. Protein concentrations were determined using Roti-Quant Bradford reagent (Carl Roth, cat. no. K015.3) against a calibration curve generated with BSA as a standard. The absorbance values were measured at 595 nm in a BioPhotometer Plus (Eppendorf, Germany). 5 µg of each nuclear extract sample was then analyzed using a NF-κB (p65) Transcription Factor Assay Kit (Cayman Chemicals, cat. no. 10007889). In brief, samples were incubated with a specific double stranded DNA oligonucleotide containing the NF-κB response element, which was immobilized on a 96-well plate. After washing, the NF-κB-containing complexes which bound to the immobilized DNA were detected using a specific primary antibody directed against NF-κB (p65). In some experiments, CREB-binding protein as a component of the NF-κB transcription factor complex was detected instead, using anti-CBP Antibody (Santa Cruz Biotechnology, cat. no. sc-583), at a 1:100 dilution. A secondary antibody conjugated to HRP was added to provide a colorimetric readout at 450 nm. The absorbance values were measured in a PolarStar plate reader (BMG Labtech, Germany). Specificity of the binding was verified by adding 10 µL of the NF-κB response element oligonucleotide solution (GGGACTTTCC, provided by the manufacturer), in a final volume of 100 µL, during the incubation with nuclear extracts.

Metabolic Stability Assay. The assay was performed with liver microsomes from male Sprague-Dawley rats (BD Bioscience, Catalog # 452501) exactly as described previously.[58]

***In vivo* Pharmacokinetic study.** Female NMRI nu/nu mice (weight 28-32 g, Janvier, France) were used. The animals were housed in a temperature-controlled room (20-24°C) and maintained in a 12 h light/12 h dark cycle. Food and water were available ad libitum. For each test compound, nine animals were used. All experimental procedures were approved by and conducted in accordance with the regulations of the local Animal Welfare authorities. Compounds were formulated in PBS/propylene glycol (80:20, v/v) at a concentration of 1 mg/mL using ultra-sonication. After subcutaneous application (10 mg/kg dose), blood samples (two per animal) were taken at 10 minutes, 30 minutes, 1, 3, 8 and 24 hours. The blood was collected in heparinized tubes, stored on ice and subsequently centrifuged at 3000 g for 10 min at 4°C. The plasma was prepared within 45 min after sampling and was kept at -20 °C until being assayed. A 20 µL aliquot of plasma sample was subjected to protein precipitation using 40 µL of acetonitrile containing 600 ng/mL of internal standard (griseofulvin). Samples were vigorously shaken and centrifuged for 10 minutes at 6.000 g and 20 °C. The particle free supernatant was diluted 1:1 with water. An aliquot was transferred to 200 µL sampler vials and subsequently subjected to LC-MS with an injection volume of 18 µL. The LC-MS system consisted of a Surveyor MS Plus HPLC system (Thermo Fisher Scientific) connected to a TSQ Quantum Discovery Max (Thermo Fisher Scientific) triple quad mass spectrometer; data handling and analysis was done using the standard software Xcalibur 2.0.7. The compound concentrations were quantified using a calibration curve based on calibration standards prepared in drug-free plasma.

***In vivo* tumor xenograft study.** MDA-MB-231 tumor cells suspended in Matrigel ($2x10^6$ cells per site in 100 µL) were injected in the left and right flank of female NMRI nu/nu mice (~8 weeks of age). Five days after the inoculation, the treatment was started (= day 1, 6 mice per

group). Compounds were formulated as described above for the pharmacokinetic study and injected s.c.. The animals were treated with compounds or vehicle for 14 days every week day. Then the treatment was paused for 6 days due to the occurrence of some precipitate under the skin. From day 21, the treatment was continued on every second day until the mice were sacrificed (day 28). Tumor size was analyzed by calipers (smallest and largest diameter) once a week, starting on the first day. Statistical significance between each compound–treated and the vehicle–treated group was calculated using the unpaired two-tailed Student´s t-test.

ASSOCIATED CONTENT

Supporting Information

The Supporting Information is available free of charge on the ACS Publications website at DOI: Complete set of screened compounds (Chart S1); Supporting Tables S1–S4; Supporting Figures S1–S4; Experimental details; Molecular Formula Strings Table

AUTHOR INFORMATION

Corresponding Author

*Tel: +49 681 302 70312. Fax: +49 681 302 70308. E-mail: ma.engel@mx.uni-saarland.de.

Notes

The authors declare no competing financial interest.

ACKNOWLEDGMENTS

We thank Mrs. Nadja Weber for her excellent work with the reporter gene and metabolic stability assays.

ABBREVIATIONS

CBP, CREB-binding protein; RIPK-2, Receptor-interacting serine/threonine-protein kinase 2; CHO, chinese hamster ovary cells; HUVEC, human umbilical vein endothelial cells; Pim-1, proto-oncogenic serine/threonine-protein kinase PIM1; Mnk, MAP kinase-interacting serine/threonine-protein kinase; SIK2, Salt-Inducible Serine/Threonine Kinase 2; LOK/STK10, Lymphocyte-Oriented Kinase; HER, human epidermal growth factor receptor; EPHA6, Ephrin Type-A Receptor 6

FUNDING

We would like to thank the Deutsche Forschungsgemeinschaft (DFG) for financial support to M.E. (grant no. EN 381/2-3). We are also grateful both to the Deutscher Akademischer Austauschdienst (DAAD) (grant no. 56607676) and the Science and Technology Development Fund (STDF), Egypt (grant no. 3579), for the support of M.M.H. and S.S.D.

REFERENCES

(1) Sharma, S. V.; Bell, D. W.; Settleman, J.; Haber, D. A. Epidermal growth factor receptor mutations in lung cancer. *Nat. Rev. Cancer* **2007,** 7, 169-181.

(2) Sequist, L. V.; Lynch, T. J. EGFR tyrosine kinase inhibitors in lung cancer: an evolving story. *Annu. Rev. Med.* **2008,** 59, 429-442.

(3) da Cunha Santos, G.; Shepherd, F. A.; Tsao, M. S. EGFR mutations and lung cancer. *Annu. Rev. Pathol.* **2011,** 6, 49-69.

(4) Godin-Heymann, N.; Ulkus, L.; Brannigan, B. W.; McDermott, U.; Lamb, J.; Maheswaran, S.; Settleman, J.; Haber, D. A. The T790M "gatekeeper" mutation in EGFR mediates resistance to low concentrations of an irreversible EGFR inhibitor. *Mol. Cancer Ther.* **2008,** 7, 874-879.

(5) Engelman, J. A.; Zejnullahu, K.; Mitsudomi, T.; Song, Y.; Hyland, C.; Park, J. O.; Lindeman, N.; Gale, C. M.; Zhao, X.; Christensen, J.; Kosaka, T.; Holmes, A. J.; Rogers, A. M.; Cappuzzo, F.; Mok, T.; Lee, C.; Johnson, B. E.; Cantley, L. C.; Janne, P. A. MET amplification leads to gefitinib resistance in lung cancer by activating ERBB3 signaling. *Science* **2007,** 316, 1039-1043.

(6) Duffy, M. J.; McGowan, P. M.; Crown, J. Targeted therapy for triple-negative breast cancer: where are we? *Int. J. Cancer* **2012,** 131, 2471-2477.

(7) deFazio, A.; Chiew, Y. E.; McEvoy, M.; Watts, C. K.; Sutherland, R. L. Antisense estrogen receptor RNA expression increases epidermal growth factor receptor gene expression in breast cancer cells. *Cell Growth Differ.* **1997,** 8, 903-911.

(8) Nielsen, T. O.; Hsu, F. D.; Jensen, K.; Cheang, M.; Karaca, G.; Hu, Z.; Hernandez-Boussard, T.; Livasy, C.; Cowan, D.; Dressler; Akslen, L. A.; Ragaz, J.; Gown, A. M.; Gilks, C.

B.; van de Rijn, M.; Perou, C. M. Immunohistochemical and clinical characterization of the basal-like subtype of invasive breast carcinoma. *Clin. Cancer Res.* **2004,** 10, 5367-5374.

(9) Corkery, B.; Crown, J.; Clynes, M.; O'Donovan, N. Epidermal growth factor receptor as a potential therapeutic target in triple-negative breast cancer. *Ann. Oncol.* **2009,** 20, 862-867.

(10) Nakai, K.; Hung, M. C.; Yamaguchi, H. A perspective on anti-EGFR therapies targeting triple-negative breast cancer. *Am. J. Cancer Res.* **2016,** 6, 1609-1623.

(11) Biswas, D. K.; Cruz, A. P.; Gansberger, E.; Pardee, A. B. Epidermal growth factor-induced nuclear factor κB activation: a major pathway of cell-cycle progression in estrogen-receptor negative breast cancer cells. *Proc. Natl. Acad. Sci. U S A.* **2000,** 97, 8542-8547.

(12) Nakshatri, H.; Bhat-Nakshatri, P.; Martin, D. A.; Goulet, R. J.; Sledge, G. W. J. Constitutive activation of NF-kB during progression of breast cancer to hormone-independent growth. *Mol. Cell. Biol.* **1997,** 17, 3629-3639.

(13) Shostak, K.; Chariot, A. EGFR and NF-kappaB: partners in cancer. *Trends Mol. Med.* **2015,** 21, 385-393.

(14) Bivona, T. G.; Hieronymus, H.; Parker, J.; Chang, K.; Taron, M.; Rosell, R.; Moonsamy, P.; Dahlman, K.; Miller, V. A.; Costa, C.; Hannon, G.; Sawyers, C. L. FAS and NF-kappaB signalling modulate dependence of lung cancers on mutant EGFR. *Nature* **2011,** 471, 523-526.

(15) Blakely, C. M.; Pazarentzos, E.; Olivas, V.; Asthana, S.; Yan, J. J.; Tan, I.; Hrustanovic, G.; Chan, E.; Lin, L.; Neel, D. S.; Newton, W.; Bobb, K. L.; Fouts, T. R.; Meshulam, J.; Gubens, M. A.; Jablons, D. M.; Johnson, J. R.; Bandyopadhyay, S.; Krogan, N. J.; Bivona, T. G. NF-kappaB-activating complex engaged in response to EGFR oncogene inhibition drives tumor cell survival and residual disease in lung cancer. *Cell Rep.* **2015,** 11, 98-110.

(16) Shimizu, T.; Tolcher, A. W.; Papadopoulos, K. P.; Beeram, M.; Rasco, D. W.; Smith, L. S.; Gunn, S.; Smetzer, L.; Mays, T. A.; Kaiser, B.; Wick, M. J.; Alvarez, C.; Cavazos, A.; Mangold, G. L.; Patnaik, A. The clinical effect of the dual-targeting strategy involving PI3K/AKT/mTOR and RAS/MEK/ERK pathways in patients with advanced cancer. *Clin. Cancer Res.* **2012,** 18, 2316-2325.

(17) Rewcastle, G. W.; Denny, W. A.; Bridges, A. J.; Zhou, H.; Cody, D. R.; McMichael, A.; Fry, D. W. Tyrosine kinase inhibitors. 5. Synthesis and structure-activity relationships for 4-[(phenylmethyl)amino]- and 4-(phenylamino)quinazolines as potent adenosine 5'-triphosphate binding site inhibitors of the tyrosine kinase domain of the epidermal growth factor receptor. *J. Med. Chem.* **1995,** 38, 3482-3487.

(18) Smaill, J. B.; Rewcastle, G. W.; Loo, J. A.; Greis, K. D.; Chan, O. H.; Reyner, E. L.; Lipka, E.; Showalter, H. D.; Vincent, P. W.; Elliott, W. L.; Denny, W. A. Tyrosine kinase inhibitors. 17. Irreversible inhibitors of the epidermal growth factor receptor: 4-(phenylamino)quinazoline- and 4-(phenylamino)pyrido[3,2-d]pyrimidine-6-acrylamides bearing additional solubilizing functions. *J. Med. Chem.* **2000,** 43, 1380-1397.

(19) Sajan, M. P.; Nimal, S.; Mastorides, S.; Acevedo-Duncan, M.; Kahn, C. R.; Fields, A. P.; Braun, U.; Leitges, M.; Farese, R. V. Correction of metabolic abnormalities in a rodent model of obesity, metabolic syndrome, and type 2 diabetes mellitus by inhibitors of hepatic protein kinase C-iota. *Metabolism* **2012,** 61, 459-469.

(20) Jones, T. R.; Thornton, T. J.; Flinn, A.; Jackman, A. L.; Newell, D. R.; Calvert, A. H. Quinazoline antifolates inhibiting thymidylate synthase: 2-desamino derivatives with enhanced solubility and potency. *J. Med. Chem.* **1989,** 32, 847-852.

(21) Cavalli, A.; Lizzi, F.; Bongarzone, S.; Brun, R.; Luise Krauth-Siegel, R.; Bolognesi, M. L. Privileged structure-guided synthesis of quinazoline derivatives as inhibitors of trypanothione reductase. *Bioorg. Med. Chem. Lett.* **2009,** 19, 3031-3035.

(22) Takase, Y.; Saeki, T.; Watanabe, N.; Adachi, H.; Souda, S.; Saito, I. Cyclic GMP phosphodiesterase inhibitors. 2. Requirement of 6-substitution of quinazoline derivatives for potent and selective inhibitory activity. *J. Med. Chem.* **1994,** 37, 2106-2111.

(23) Berra, E.; Diaz-Meco, M. T.; Lozano, J.; Frutos, S.; Municio, M. M.; Sanchez, P.; Sanz, L.; Moscat, J. Evidence for a role of MEK and MAPK during signal transduction by protein kinase C zeta. *Embo. J.* **1995,** 14, 6157-6163.

(24) Marugan, J. J.; Zheng, W.; Motabar, O.; Southall, N.; Goldin, E.; Westbroek, W.; Stubblefield, B. K.; Sidransky, E.; Aungst, R. A.; Lea, W. A.; Simeonov, A.; Leister, W.; Austin, C. P. Evaluation of quinazoline analogues as glucocerebrosidase inhibitors with chaperone activity. *J. Med. Chem.* **2011,** 54, 1033-1058.

(25) Levy, D.; Kuo, A. J.; Chang, Y.; Schaefer, U.; Kitson, C.; Cheung, P.; Espejo, A.; Zee, B. M.; Liu, C. L.; Tangsombatvisit, S.; Tennen, R. I.; Kuo, A. Y.; Tanjing, S.; Cheung, R.; Chua, K. F.; Utz, P. J.; Shi, X.; Prinjha, R. K.; Lee, K.; Garcia, B. A.; Bedford, M. T.; Tarakhovsky, A.; Cheng, X.; Gozani, O. Lysine methylation of the NF-kappaB subunit RelA by SETD6 couples activity of the histone methyltransferase GLP at chromatin to tonic repression of NF-kappaB signaling. *Nat. Immunol.* **2011,** 12, 29-36.

(26) Evans, B. E.; Rittle, K. E.; Bock, M. G.; DiPardo, R. M.; Freidinger, R. M.; Whitter, W. L.; Lundell, G. F.; Veber, D. F.; Anderson, P. S.; Chang, R. S.; Lotti, V. J.; Cerino, D. J.; Chen, T. B.; Kling P. J.; Kunkel K. A.; Springer J. P.; Hirshfield J. Methods for drug discovery:

development of potent, selective, orally effective cholecystokinin antagonists. *J. Med. Chem.* **1988,** 31, 2235-2246.

(27) Hamed, M. M.; Abou El Ella, D. A.; Keeton, A. B.; Piazza, G. A.; Engel, M.; Hartmann, R. W.; Abadi, A. H. Quinazoline and tetrahydropyridothieno[2,3-d]pyrimidine derivatives as irreversible EGFR tyrosine kinase inhibitors: influence of the position 4 substituent. *Med. Chem. Commun.* **2013,** 4, 1202-1207.

(28) Hamed, M. M.; Abou El Ella, D. A.; Keeton, A. B.; Piazza, G. A.; Abadi, A. H.; Hartmann, R. W.; Engel, M. 6-Aryl and heterocycle quinazoline derivatives as potent EGFR inhibitors with improved activity toward gefitinib-sensitive and -resistant tumor cell lines. *ChemMedChem* **2013,** 8, 1495-504.

(29) Passmore, J. S.; Lukey, P. T.; Ress, S. R. The human macrophage cell line U937 as an in vitro model for selective evaluation of mycobacterial antigen-specific cytotoxic T-cell function. *Immunology* **2001,** 102, 146-156.

(30) Tobe, M.; Isobe, Y.; Tomizawa, H.; Nagasaki, T.; Takahashi, H.; Fukazawa, T.; Hayashi, H. Discovery of quinazolines as a novel structural class of potent inhibitors of NF-kappa B activation. *Bioorg. Med. Chem.* **2003,** 11, 383-391.

(31) Tobe, M.; Isobe, Y.; Tomizawa, H.; Nagasaki, T.; Takahashi, H.; Hayashi, H. A novel structural class of potent inhibitors of NF-kappa B activation: structure-activity relationships and biological effects of 6-aminoquinazoline derivatives. *Bioorg. Med. Chem.* **2003,** 11, 3869-3878.

(32) Haas, T. L.; Emmerich, C. H.; Gerlach, B.; Schmukle, A. C.; Cordier, S. M.; Rieser, E.; Feltham, R.; Vince, J.; Warnken, U.; Wenger, T.; Koschny, R.; Komander, D.; Silke, J.; Walczak, H. Recruitment of the linear ubiquitin chain assembly complex stabilizes the TNF-R1

signaling complex and is required for TNF-mediated gene induction. *Mol. Cell* **2009,** 36, 831-844.

(33) Golan-Goldhirsh, A.; Gopas, J. Plant derived inhibitors of NF-κB. *Phytochem. Rev.* **2014,** 13, 107-121.

(34) Fan, W. H.; Lu, Y. L.; Deng, F.; Ge, X. M.; Liu, S.; Tang, P. H. EGFR antisense RNA blocks expression of the epidermal growth factor receptor and partially reverse the malignant phenotype of human breast cancer MDA-MB-231 cells. *Cell Res.* **1998,** 8, 63-71.

(35) Ferrer-Soler, L.; Vazquez-Martin, A.; Brunet, J.; Menendez, J. A.; De Llorens, R.; Colomer, R. An update of the mechanisms of resistance to EGFR-tyrosine kinase inhibitors in breast cancer: gefitinib (Iressa) -induced changes in the expression and nucleo-cytoplasmic trafficking of HER-ligands (Review). *Int. J. Mol. Med.* **2007,** 20, 3-10.

(36) Sovak, M. A.; Bellas, R. E.; Kim, D. W.; Zanieski, G. J.; Rogers, A. E.; Traish, A. M.; Sonenshein, G. E. Aberrant nuclear factor-kappaB/Rel expression and the pathogenesis of breast cancer. *J. Clin. Invest.* **1997,** 100, 2952-2960.

(37) Anastassiadis, T.; Deacon, S. W.; Devarajan, K.; Ma, H.; Peterson, J. R. Comprehensive assay of kinase catalytic activity reveals features of kinase inhibitor selectivity. *Nat. Biotechnol.* **2011,** 29, 1039-1045.

(38) Beharry, Z.; Zemskova, M.; Mahajan, S.; Zhang, F.; Ma, J.; Xia, Z.; Lilly, M.; Smith, C. D.; Kraft, A. S. Novel benzylidene-thiazolidine-2,4-diones inhibit Pim protein kinase activity and induce cell cycle arrest in leukemia and prostate cancer cells. *Mol. Cancer Ther.* **2009,** 8, 1473-1483.

(39) Palombella, V. J.; Rando, O. J.; Goldberg, A. L.; Maniatis, T. The ubiquitin-proteasome pathway is required for processing the NF-kB1 precursor protein and the activation of NF-kB. *Cell* **1994,** 78, 773-785.

(40) Montagut, C.; Rovira, A.; Mellado, B.; Gascon, P.; Ross, J. S.; Albanell, J. Preclinical and clinical development of the proteasome inhibitor bortezomib in cancer treatment. *Drugs Today (Barc)* **2005,** 41, 299-315.

(41) Berkers, C. R.; Verdoes, M.; Lichtman, E.; Fiebiger, E.; Kessler, B. M.; Anderson, K. C.; Ploegh, H. L.; Ovaa, H.; Galardy, P. J. Activity probe for in vivo profiling of the specificity of proteasome inhibitor bortezomib. *Nat. Methods* **2005,** 2, 357-362.

(42) Hayden, M. S.; Ghosh, S. Signaling to NF-kappaB. *Genes Dev.* **2004,** 18, 2195-2224.

(43) Yang, J.; Jiang, H.; Chen, S. S.; Chen, J.; Xu, S. K.; Li, W. Q.; Wang, J. C. CBP knockdown inhibits angiotensin II-induced vascular smooth muscle cells proliferation through downregulating NF-kB transcriptional activity. *Mol. Cell Biochem.* **2010,** 340, 55-62.

(44) Ma, B.; Fey, M.; Hottiger, M. O. WNT/beta-catenin signaling inhibits CBP-mediated RelA acetylation and expression of proinflammatory NF-kappaB target genes. *J. Cell Sci.* **2015,** 128, 2430-2436.

(45) Hua, B.; Tamamori-Adachi, M.; Luo, Y.; Tamura, K.; Morioka, M.; Fukuda, M.; Tanaka, Y.; Kitajima, S. A splice variant of stress response gene ATF3 counteracts NF-kappaB-dependent anti-apoptosis through inhibiting recruitment of CREB-binding protein/p300 coactivator. *J. Biol. Chem.* **2006,** 281, 1620-1629.

(46) Mukherjee, S. P.; Behar, M.; Birnbaum, H. A.; Hoffmann, A.; Wright, P. E.; Ghosh, G. Analysis of the RelA:CBP/p300 interaction reveals its involvement in NF-kappaB-driven transcription. *PLoS Biol.* **2013,** 11, e1001647.

(47) Tilstra, J. S.; Gaddy, D. F.; Zhao, J.; Dave, S. H.; Niedernhofer, L. J.; Plevy, S. E.; Robbins, P. D. Pharmacologic IKK/NF-kappaB inhibition causes antigen presenting cells to undergo TNFalpha dependent ROS-mediated programmed cell death. *Sci. Rep.* **2014,** 4, 3631.

(48) Verstrepen, L.; Beyaert, R. Receptor proximal kinases in NF-kappaB signaling as potential therapeutic targets in cancer and inflammation. *Biochem Pharmacol* **2014,** 92, 519-29.

(49) Enzler, T.; Sano, Y.; Choo, M. K.; Cottam, H. B.; Karin, M.; Tsao, H.; Park, J. M. Cell-selective inhibition of NF-kappaB signaling improves therapeutic index in a melanoma chemotherapy model. *Cancer Discovery* **2011,** 1, 496-507.

(50) Aggarwal, B. B.; Sung, B. NF-kappaB in cancer: a matter of life and death. *Cancer Discovery* **2011,** 1, 469-471.

(51) Picaud, S.; Fedorov, O.; Thanasopoulou, A.; Leonards, K.; Jones, K.; Meier, J.; Olzscha, H.; Monteiro, O.; Martin, S.; Philpott, M.-.; Tumber, A.; Filippakopoulos, P.; Yapp, C.; Wells, C.; Che, K. H.; Bannister, A.; Robson, S.; Kumar, U.-.; Parr, N.; Lee, K.; Lugo, D.; Jeffrey, P.; Taylor, S.; Vecellio, L. M.; Bountra, C.; Brennan, P.-.; O'Mahony, A.; Velichko, S.; Müller, S.; Hay, D.; Daniels, D. L.; Urh, M.; La Thangue, N. B.; Kouzarides, T.; Prinjha, R.; Schwaller, J.; Knapp, S. Generation of a selective small molecule inhibitor of the CBP/p300 bromodomain for leukemia therapy. *Cancer Res.* **2015,** 75, 5106-5119.

(52) Dancy, B. M.; Cole, P. A. Protein Lysine Acetylation by p300/CBP. *Chem. Rev.* **2015,** 115, 2419-2452.

(53) Naruse, I.; Ohmori, T.; Ao, Y.; Fukumoto, H.; Kuroki, T.; Mori, M.; Saijo, N.; Nishio, K. Antitumor activity of the selective epidermal growth factor receptor-tyrosine kinase inhibitor (EGFR-TKI) Iressa® (ZD1839) in an EGFR-expressing multidrug-resistant cell line in vitro and in vivo. *Int. J. Cancer* **2002,** 98, 310-315.

(54) Barker, A. J.; Gibson, K. H.; Grundy, W.; Godfrey, A. A.; Barlow, J. J.; Healy, M. P.; Woodburn, J. R.; Ashton, S. E.; Curry, B. J.; Scarlett, L.; Henthorn, L.; Richards, L. Studies leading to the identification of ZD1839 (IressaTM): an orally active, selective epidermal growth factor receptor tyrosine kinase inhibitor targeted to the treatment of cancer. *Biorog. Med. Chem. Lett.* **2001,** 11, 1911-1914.

(55) Choi, S. Y.; Lin, D.; Gout, P. W.; Collins, C. C.; Xu, Y.; Wang, Y. Lessons from patient-derived xenografts for better in vitro modeling of human cancer. *Adv. Drug Deliv. Rev.* **2014,** 79-80, 222-237.

(56) Fry, D. W.; Kraker, A. J.; McMichael, A.; Ambroso, L. A.; Nelson, J. M.; Leopold, W. R.; Connors, R. W.; Bridges, A. J. A specific inhibitor of the epidermal growth factor receptor tyrosine kinase. *Science* **1994,** 265, 1093-1095.

(57) Frohner, W.; Lopez-Garcia, L. A.; Neimanis, S.; Weber, N.; Navratil, J.; Maurer, F.; Stroba, A.; Zhang, H.; Biondi, R. M.; Engel, M. 4-benzimidazolyl-3-phenylbutanoic acids as novel PIF-pocket-targeting allosteric inhibitors of protein kinase PKCzeta. *J. Med. Chem.* **2011,** 54, 6714-6723.

(58) Schmitt, C.; Kail, D.; Mariano, M.; Empting, M.; Weber, N.; Paul, T.; Hartmann, R. W.; Engel, M. Design and synthesis of a library of lead-like 2,4-bisheterocyclic substituted thiophenes as selective Dyrk/Clk inhibitors. *PLoS One* **2014,** 9, e87851.

FIGURES

Figure 1

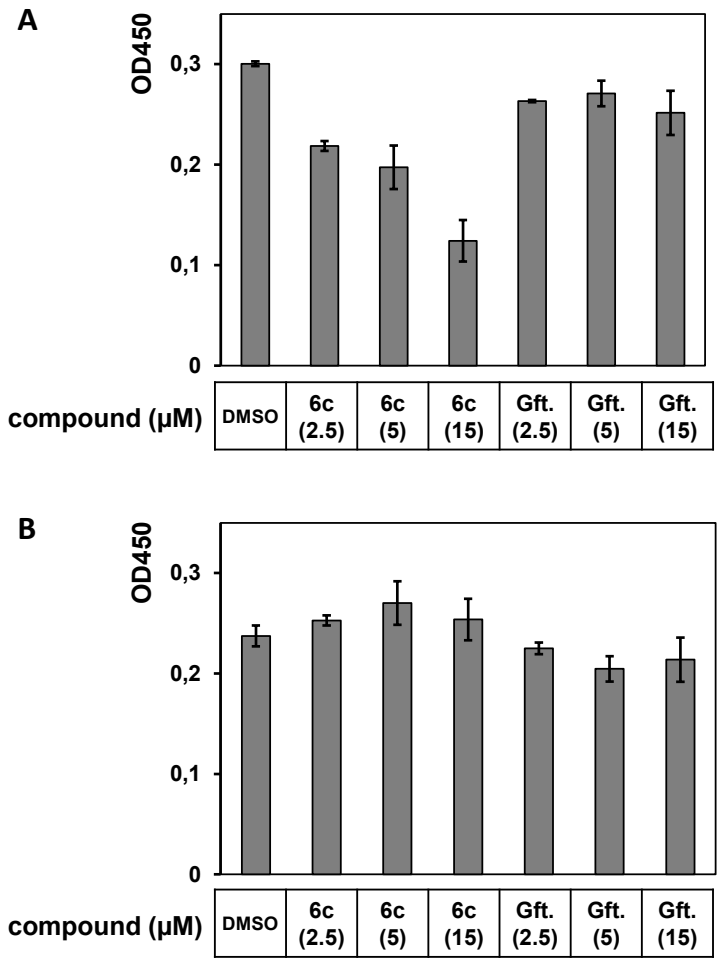

Figure 2

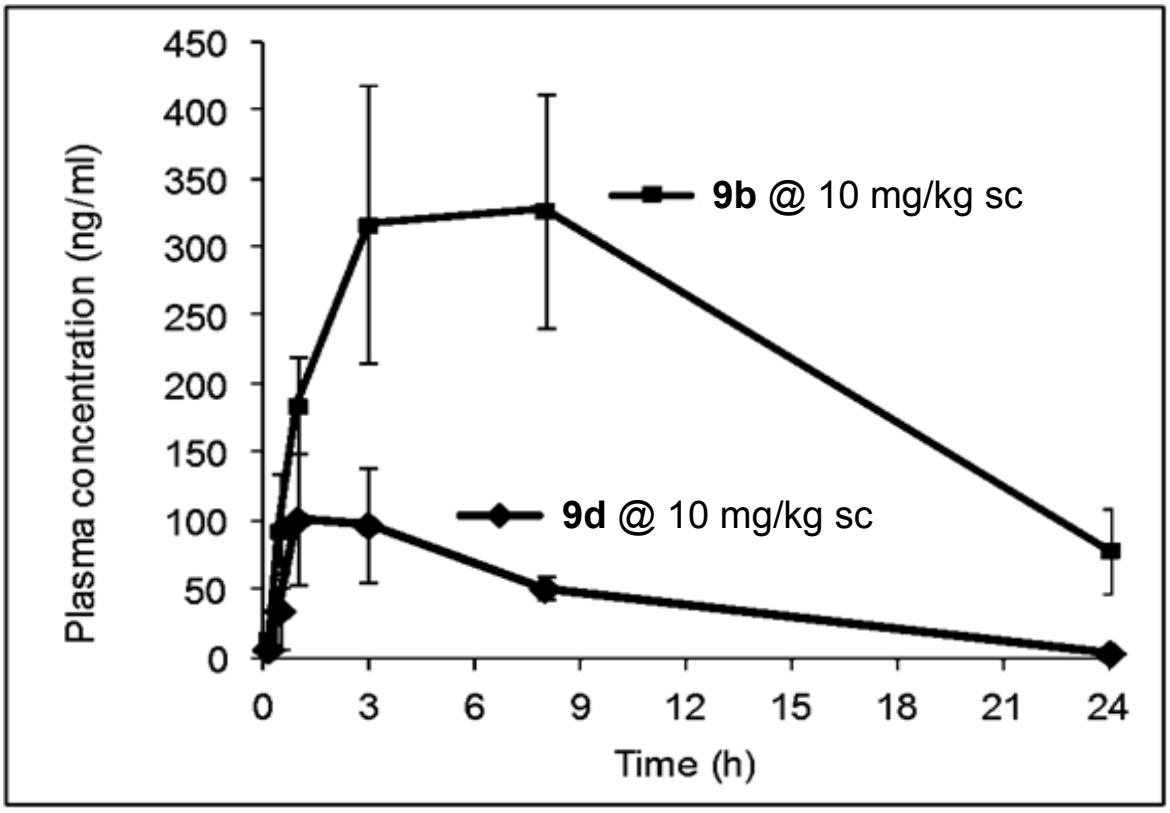
Plasma concentration (ng/ml)
450
400
350
300
250
200
150
100
50
0
0
3
6
9
12
15
18
21
24
Time (h)
9b @ 10 mg/kg sc
9d @ 10 mg/kg sc

Figure 3

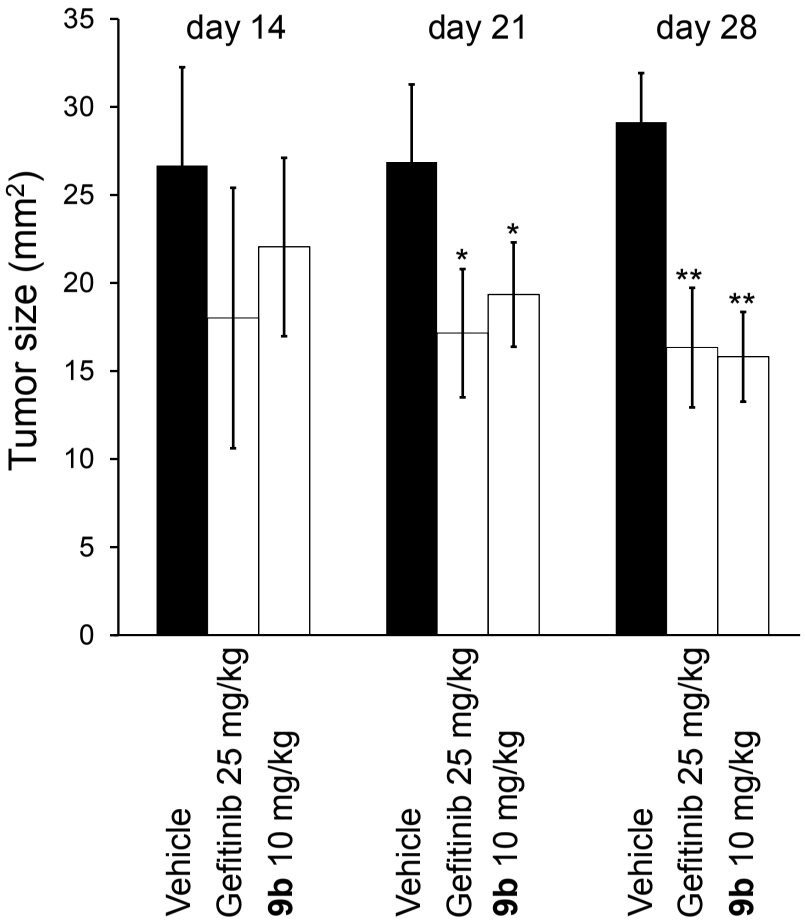
day 14
day 21
day 28
Tumor size (mm2)
35
30
25
20
15
10
5
0
*
*
**
**
Vehicle
Gefitinib 25 mg/kg
9b 10 mg/kg
Vehicle
Gefitinib 25 mg/kg
9b 10 mg/kg
Vehicle
Gefitinib 25 mg/kg
9b 10 mg/kg

FIGURE LEGENDS

Figure 1. Compound **6c** but not gefitinib reduces the amount of CREB-binding protein (CBP) in the NF-κB transcription complex. MDA-MB-231 cells were treated with compounds or DMSO for 12 h as indicated (in backets: concentration in μM). 5 μg of isolated nuclear proteins were analyzed for the specific binding to the NF-κB response element oligonucleotide on an ELISA plate. **A.** CBP physically associated with bound RelA/p65 was detected using a specific primary antibody directed against CBP, followed by a HRP-coupled secondary antibody and colorimetric reaction. **B.** The same nuclear extracts as in A were analyzed in parallel, however, anti-RelA/p65 was used as a primary antibody. OD450, optical density at 450 nm; Gft., gefitinib. The experiment was performed in triplicates; error bars indicate the S.D. values. One representative experiment out of three is shown, which essentially gave the same results.

Figure 2. Time–dependent plasma concentrations of **9b** and **9d** after subcutaneous administration to female NMRI nu/nu mice.

Figure 3. 9b inhibits tumor growth in a xenograft model. MDA-MB-231 tumor cells were injected in female NMRI nu/nu mice, and the treatment with the test compounds or vehicle started five days after the inoculation (day 1) as described under Experimental. Mean values of the measured tumor sizes are shown (error bars: ± S.D.). The asterisks denote statistical significance compared with the vehicle–treated group: *, $p< 0.05$; **, $p< 0.01$.

SCHEMES

Scheme 1.[a]

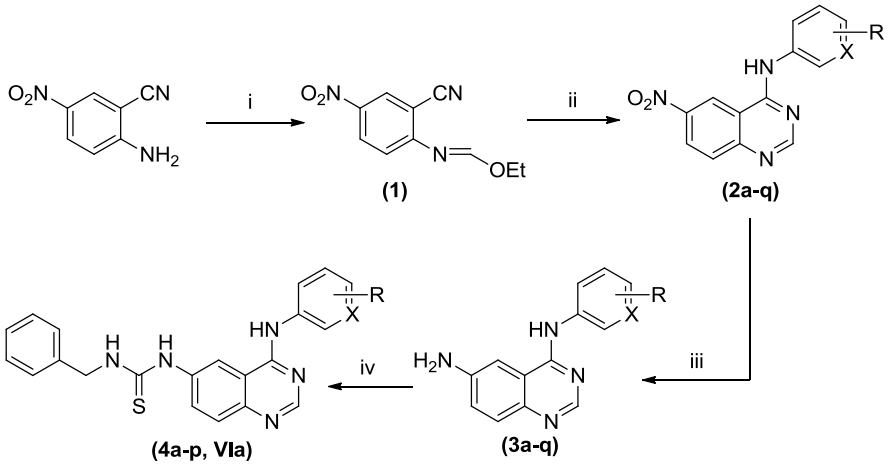

Comp.	X	R	Comp.	X	R
a	C	2-Br			
b	C	4-Br	**m**	C	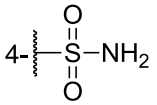
c	C	3-Cl			
d	C	3-methyl			
e	C	2,3-dimethyl	**n**	C	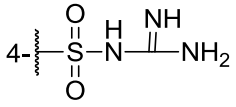
f	C	3-ethyl			
g	C	4-isopropyl			
h	C	4-t-butyl	**o**	C	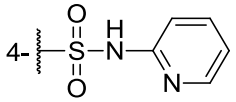
i	C	4-phenyl			
j	C	4-phenoxy	**p**	N	-
k	C	3-OH	**q, VIa**	C	3-Br
l	C	4-OH			

[a]Reagents and conditions: (i) TEOF, $(Ac)_2O$, reflux, 16h; (ii) R-NH_2, CH_3COOH, reflux, 1h; (iii) $SnCl_2$, MeOH, reflux, 30 min; (iv) $PhCH_2$-NCS, DMF, rt, 5h.

Scheme 2.[a]

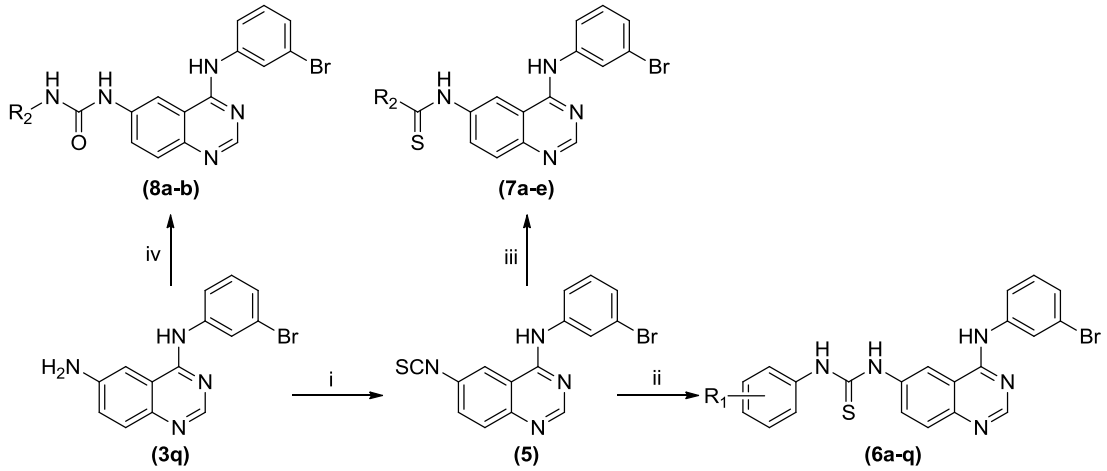

Comp.	R_1	Comp.	R_2
6a	H	**7a**	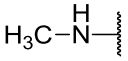
6b	2-Cl		
6c	3-Cl	**7b**	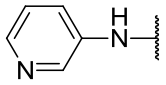
6d	4-Cl		
6e	4-OH		
6f	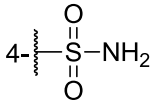		
6g	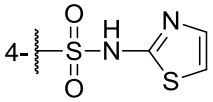	**7c**	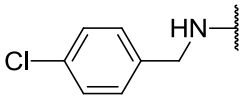
6h	3-Cl,4-F		
6i	3-CF_3,4-Cl		
6j	2-F,3-CF_3	**7d**	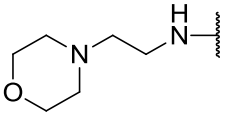
6k	4-CF_3		
6l	3-CF_3		
6m	3,5-di-trifluoromethyl	**7e**	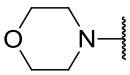
6n	4-Br		
6o	2,4-dichloro		
6p	3,4-dichloro	**8a**	benzyl
6q	3,5-dichloro	**8b**	4-chlorophenyl

[a]Reagents and conditions: (i) $S{=}CCl_2$, HCl (ii)Ar-NH_2, DMF, rt, 5h (iii) R-NH_2, DMF, rt, 5h (iv) R-NCO, DMF, rt, 5h

Scheme 3.[a]

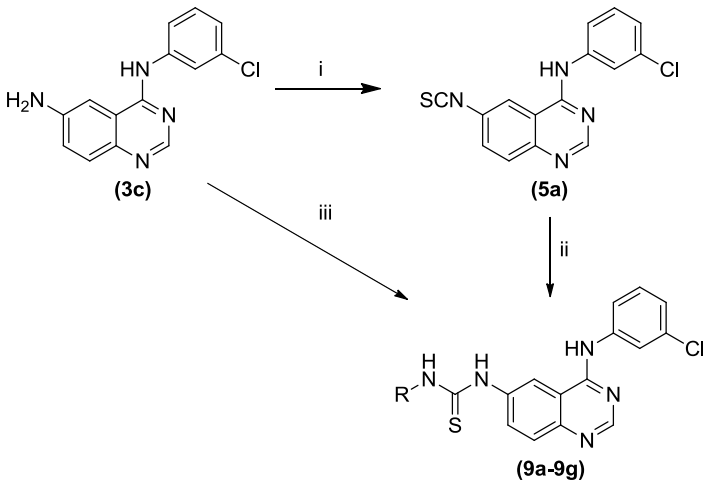

[a]Reagents and conditions: (i) $S{=}CCl_2$, HCl (ii) Ar-NH_2, DMF, rt, 5h "used for 9a-9c" (iii) PhOCSCl, Ar-NH_2, DMF, 1h "used for 9d-9g"

Comp.	R	Comp.	R
9a	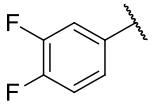	**9e**	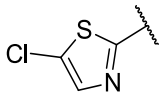
9b	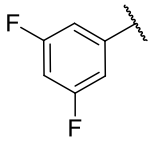	**9f**	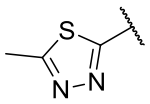
9c	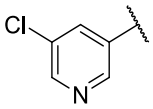	**9g**	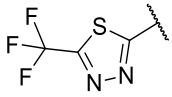
9d	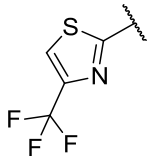		

CHARTS

Chart 1. General structures of the quinazoline derivatives selected for screening towards the NF-κB inhibitory activity.

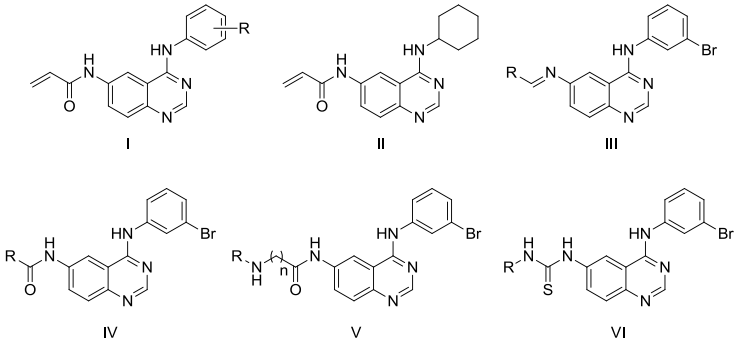

Chart 2. Overview on the modifications of hit compound **VIa.**

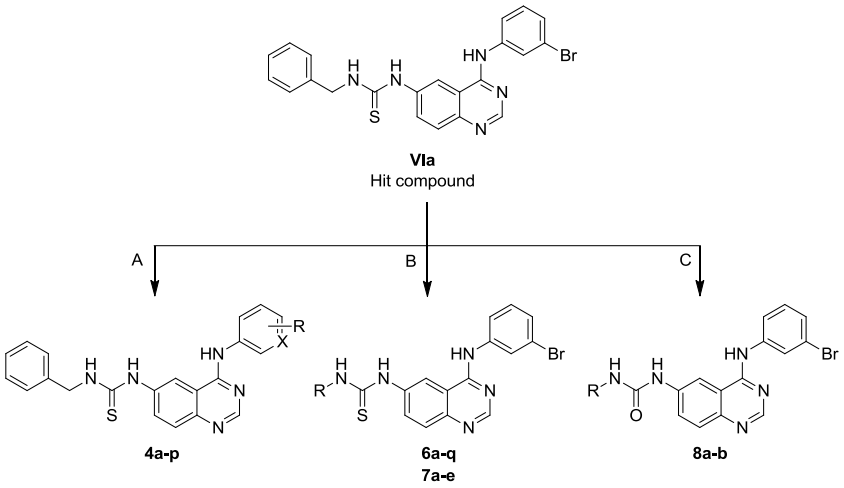

TABLES

Table 1. Hits of the screening of 4-Aminophenylquinazoline derivatives for dual inhibition of EGFR kinase and the NF-ţκB activation pathway

Comp.	EGFR kinase	NF-κB reporter gene assay	
	IC_{50} (nM)[a]	% inhibition[b] at 10μM	IC_{50}[b] (μM)
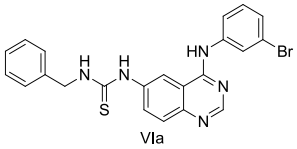 VIa	17.2	97	4.1
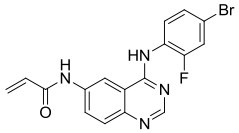 Ia	2.1	73.6	N.D.
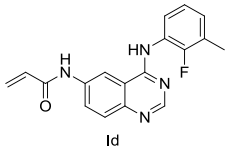 Id	1.5	70	N.D.
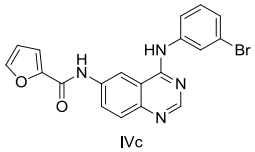 IVc	8.4	39.4	N.D.
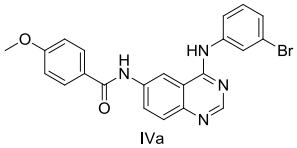 IVa	N.D.	33.2	N.D.
gefitinib	4.0	51.3	9.7

[a]Values are representative of at least two independent concentration–response experiments performed in triplicate per concentration, S.D. <8 %. [b]Results shown are means of at least two independent experiments, S.D. <14%.

Table 2. Selectivity profiling of **VIa** against the kinases associated with the TNFα receptor complex in U937 cells.[32]

Kinase	% activity at 10 μM[a]	Kinase	% activity at 10 μM[a]
IKKα(h)	117	RIPK2(h)	54
IKKβ(h)	100	SAPK2a(h)	78
PKCι(h)	106	TAK1(h)	106
PKCζ(h)	92	TBK1(h)	92

[a]Values represent the mean of two experiments, S.D. < 5 %**.** All kinases were tested using ATP concentrations at the respective K_M values.

Table 3. Biological evaluation of hit compound **VIa** derivatives modified at the 4-anilino ring

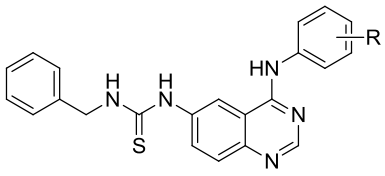

(4a-o, VIa)

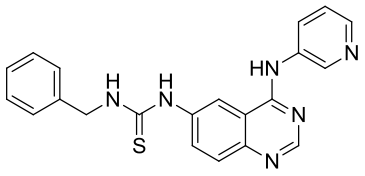

(4p)

Comp.	R	Recombinant EGFR Kinase		U937 reporter gene assay		MDA cell growth
		% inhibition at 150 nM[a]	IC_{50} (nM)[a,b]	% inhibition at 10 µM[c]	IC_{50}[c] (µM)	IC_{50}[c] (µM)
4a	2-Br	13.1	>150	85.7	6.5	>30
4b	4-Br	47.7	>150	92.1	3.8	15.1
4c	3-Cl	84.8	11.4	89.7	3.7	7.3
4d	3-methyl	68.5	36.8	76.4	N.D.	19.5
4e	2,3-dimethyl	40.0	>150	71.5	N.D.	28.7
4f	3-ethyl	41.7	>150	92.5	4.8	10.5
4g	4-isopropyl	4.2	>150	95.7	4.3	12.8
4h	4-t-butyl	0.9	>150	91.9	5.51	8.7
4i	4-phenyl	14.5	>150	89.1	4.4	8.4
4j	4-phenoxy	21.9	>150	73.7	N.D.	6.8
4k	3-OH	60.8	63.6	44.3	N.D.	>30
4l	4-OH	44.1	>150	24.1	N.D.	27
4m	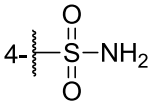	17.7	>150	19.2	N.D.	>30
4n	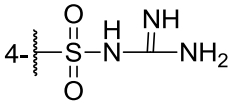	6.7	>150	21.7	N.D.	>30
4o	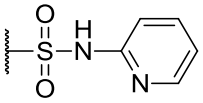	20.9	>150	6.6	N.D.	>30
4p	-	38.5	>150	7.7	N.D.	17.9
VIa	3-Br	86.1	17.2	97	4.1	9.5

[a]Values are representative of at least two independent concentration–response experiments performed in triplicate per concentration, S.D. <8 %. [b]IC_{50}s were determined for the compounds showing at least 50% inhibition at 150 nM. [c]Results shown are means of at least two independent experiments, S.D. <12%.

Table 4. Biological evaluation of hit compound **VIa** derivatives modified at position 6 of the quinazoline

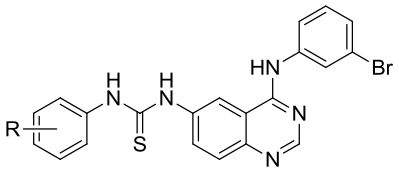
(6a-q)

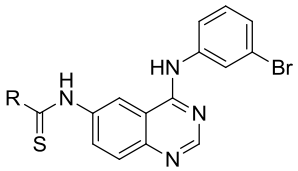
(7a-e)

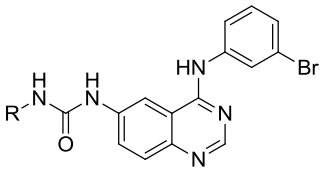
(8a-b)

Comp.	R	Recombinant EGFR Kinase		U937 reporter gene assay		MDA cell growth
		% inhibition at 150 nM[a]	IC_{50} (nM)[a,b]	% inhibition at 10μM[c]	IC_{50} (μM)[c]	IC_{50} (μM)[c]
VIa	-	86.1	17.2	97	4.1	9.5
6a	H	86.5	15.8	90.7	5.2	10.0
6b	2-Cl	84.3	15.8	95.8	3.5	8.5
6c	3-Cl	74.8	20.6	97.4	1.9	2.1
6d	4-Cl	79.6	19.5	89.5	4.9	8.2
6e	4-OH	91.5	8.9	85.3	6.4	17.3
6f	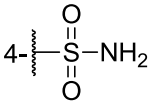	92.3	9.5	29.0	N.D.	>30
6g	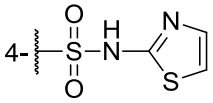	81.7	22.0	16.5	N.D.	>30
6h	3-Cl,4-F	74.1	25.3	100	1.0	0.3
6i	3-CF_3,4-Cl	44.0	>150	99.0	1.7	1.1
6j	2-F,3-CF_3	55.6	112.4	98.0	1.3	0.4
6k	4-CF_3	38.1	>150	94.8	1.7	12.2
6l	3-CF_3	57.5	60.7	96.5	1.0	1.4
6m	3,5-di-trifluoromethyl	32.3	>150	100	1.9	0.8
6n	4-Br	70.4	35.4	96.7	2.0	>30
6o	2,4-dichloro	66	48.9	93.1	2.9	12.2
6p	3,4-dichloro	52.9	133.1	97.2	1.9	4.8
6q	3,5-dichloro	50.9	146.3	99.6	1.8	3.0
7a	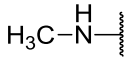	92.2	9.1	3.0	N.D.	>30
7b	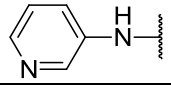	90.4	10.2	42.4	N.D.	>30

7c	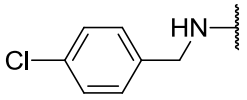	77.5	28.3	78.6	N.D.	23
7d	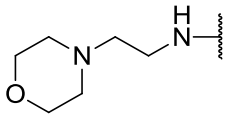	91.8	10.7	20.9	N.D.	>30
7e	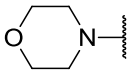	84.0	26.9	40.1	N.D.	>30
8a	benzyl	89.9	8.9	42.6	N.D.	>30
8b	4-chlorophenyl	69.0	19.3	50.3	N.D.	10
gefitinib	-	93.2	4.0	51.3	9.7	14.2

[a]Values are representative of at least two independent concentration–response experiments performed in triplicate per concentration, S.D. <8 %. [b]IC_{50}s were determined for the compounds showing at least 50 % inhibition at 150 nM. [c]Results shown are means of at least two independent experiments, S.D. <12%.

Table 5. Tumor cell–selective growth inhibition by the dual inhibitors **6c** and **6h** *vs.* gefitinib

	IC_{50} (μM)[a]				Fold selectivity CHO *vs.* tumor cell line		Fold selectivity HUVEC *vs.* tumor cell line	
Compound	**A549**	**MDA**	**CHO**	**HUVEC**	**A549**	**MDA**	**A549**	**MDA**
6c	1.6	2.1	25.7	11.5	16.1	12.2	7.2	5.5
6h	1.0	0.3	52.1	14.8	52.1	173.7	14.8	49.3
gefitinib	9.3	14.2	43.7	13.0	4.7	3.1	1.4	0.9

[a]Values are representative of three independent concentration–response experiments performed in triplicate per concentration; S.D. ≤ 12%

Table 6. Biological evaluation of the optimized dual inhibitors

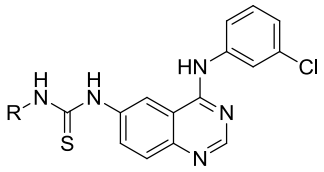

(9a-9g)

Comp.	R	U937 reporter gene assay		Recombinant EGFR Kinase	
		% inhibition at 5 μM[a]	IC_{50} (μM)[a]	% inhibition at 150 nM[b]	IC_{50} (nM)[b]
9a	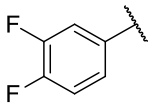	37.6	ND	44.4	ND
9b	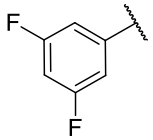	73.5	0.3	87.6	60.1
9c	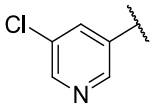	78.0	3.0	85.0	55.5
9d	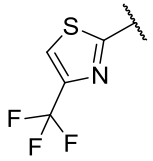	92.0	0.6	56.4	137
9e	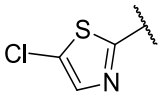	88.2	0.7	60.0	120
9f	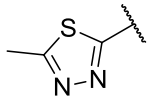	76.1	1.2	70.8	120
9g	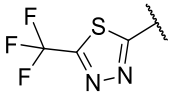	80.5	1.0	70.7	130

[a]Results shown are means of three independent experiments, S.D. <13 %. [b]Values are representative of at least two independent determinations based on triplicates per concentration, S.D. <8 %.

Table 7. Metabolic stability of **9b**, **9d** and reference compounds against rat liver microsomes[a].

Compound	Half-life [min]	Cl_{blood}[b] [mL/min/kg]
9b	139	19
9d	22	51
Diphenhydramine	17	53
Diazepam	88	27

[a]0.225 mg/mL protein, $NADP^+$-regenerating system, [inhibitor]: 0.5 µM, incubation at 37 °C, samples taken at 0, 15, 30, and 60, 90 min, determination of parent compound by MS. [b]Cl_{blood}: estimated blood clearance in rats as calculated based on *in vitro* intrinsic clearance. The values are representative for two independent experiments that essentially gave the same results.

Table 8. Pharmacokinetic parameters for **9b** and **9d**[a]

Compd.	9b	9d
C_{max} (ng/mL)	327	100.8
t_{max} (h)[b]	8.0	1.0
Concentration after 24 h (ng/mL)	79.0	3.5
$t_{1/2}$ (h)	7.8[c]	4.3
$AUC_{0\text{-}24\ h}$ (ng*h/mL)	5443	1042
$AUC_{0\text{-}\infty}$ (ng*h/mL)	6334[c]	1064
CL/f (mL/(h*kg))[d]	1578.8[c]	9401.7

[a]Single dose s.c. injection (10 mg/kg) in PBS/propylene glycol (80:20). [b]Time after drug administration needed to reach maximum plasma concentration. [c]No complete elimination phase was characterized for **9b**; thus, the values were calculated based on an estimated elimination constant. [d]Total body clearance not normalized to bioavailability.

Table of Contents graphic